FINITE ELEMENT ANALYSIS OF THERMOMECHANICAL PROBLEMS

J.H. Argyris, H. Balmer, J.St. Doltsinis, K.J. Willam

Institut für Statik und Dynamik der Luft- und Raumfahrtkonstruktionen, Universität Stuttgart
Imperial College of Science and Technology, University of London

The rate formulation for the quasistatic boundary value problem is rephrased after a brief discussion of "weak coupling" between thermal and mechanical processes. This description of the mechanical problem under non-isothermal conditions forms the basis for the subsequent finite element discretisation (matrix displacement method). First, a number of two dimensional finite element displacement models are investigated in regard to their strain approximation, bearing in mind that no thermal stresses should arise from linear temperature distributions. Subsequently, various possibilities are presented to approximate the spatial distribution of plastic work within higher order displacement models.

After this review of approximation problems, constitutive relations in thermal environments are discussed with special consideration of temperature dependent material properties.

First, the linear theory of uncoupled thermoelasticity is restated and extended to non-isothermal problems. For temperature dependent material properties there exists a fundamental difference between the hyper- and hypoelastic description of the material behaviour. Both formulations are discussed and applied to solve the thermoelastic problem of a cylinder with a spherical cavity under transient thermal conditions exhibiting temperature dependent material properties.

Subsequently, the elasto-plastic constitutive law is reformulated to incorporate a temperature dependent loading function. This general material relation is then restricted to the von Mises yield criterion and to the Prandtl-Reuss hardening rule in order to obtain quantitative thermo-elasto-plastic stress-strain relations for temperature dependent material properties. Moreover, the formulation is extended to incorporate creep effects, for which the prescribed thermal strains are supplemented by initial creep strains at the beginning of each time interval. The application of this material law to a realistic engineering example is illustrated on a pressure vessel nozzle under steady state conditions exhibiting temperature dependent material properties.

I INTRODUCTION

Highly stressed components of aircrafts, jet engines, turbines and nuclear reactors are required to perform a complex pattern of operating schedules. A common problem arises thereby due to operating schemes which give rise to rapid changes of temperature and loading and hence to local plastic deformation and associated residual stresses. Under full operation these stresses are further redistributed due to creep and relaxation.

The objective of this paper is a realistic stress analysis of structural components under steady state or transient temperature and mechanical loading conditions. At elevated temperatures most materials exhibit strain-rate sensitivity, creep, relaxation and plastic deformations at stress levels much smaller than at room temperature. These phenomena and prior deformation history have considerable effect on subsequent deformation behaviour, all of which should be considered when stresses are computed throughout the structure as function of time. Some of these aspects are accounted for within the theory of thermoelasticity, thermoplasticity and thermal creep which form the scope of this paper.

Under the assumption of quasistatic motion and weak thermomechanical coupling the solution of the thermal stress analysis reduces to two separate tasks: First, at each instant of time the temperature distribution of the structural component is determined independently of the mechanical state. Second, for these thermal conditions the stress analysis is carried out for prescribed temperature and mechanical loading conditions accounting for temperature dependence of the material properties. For the mechanical response analysis it is assumed that no distinction need to be made between deformed and undeformed configuration and that the linear strain displacement relationships provide a proper measure of deformation. For quasi-static motion it is inferred that as a result of heat conduction temperatures change so gradually that the velocities remain small.

The finite element method (matrix displacement method) provides a tool reducing the solution of complex initial value and boundary value problems of heat conduction and stress distribution to the mere application of computer programs. In the present paper this method is first applied to the determination of the transient temperature distribution for a given thermal environment which then forms the input for the subsequent thermomechanical response analysis. The main advantage of treating both problems with the finite element method is due to the fact that the same spatial discretisation can be used for the heat conduction and the associated stress analysis, reducing the preparation of input data to a minimum.

II THERMOMECHANICAL COUPLING AND HEAT CONDUCTION

The present investigation is restricted to thermomechanical processes of small deformations and slow temperature changes, in other words, only uncoupled problems are considered in which inertia effects remain negligible.

The general heat balance equation is briefly reviewed hereafter to discuss in short the assumptions in regard to thermomechanical coupling. For non-isothermal processes recourse has to be taken to the laws of thermodynamics. If the equations for conservation of mass, momentum and energy are supplemented by the proper constitutive equations of e.g. thermoelasticity the local heat balance equation may be expressed as [see 1,2] ,

$$\mathrm{Div}\,(\underset{\sim}{k}\cdot\nabla\underset{\sim}{T}) = -T\left(\frac{\partial^2\Psi}{\partial\underset{\sim}{\varepsilon}\,\partial T}:\dot{\underset{\sim}{\varepsilon}} + \frac{\partial^2\Psi}{\partial T^2}\dot{T}\right) - \rho_0 S \qquad (1)^*$$

where T denotes the absolute temperature, $\nabla\underset{\sim}{T}$ the temperature gradient, $\underset{\sim}{\varepsilon}$ the measure of total deformation, S the distributed heat source, $\underset{\sim}{k}$ the material conductivity, ρ_0 the mass density before deformation and Ψ the free energy function also called after Helmholtz. Two sources of coupling may be distinguished:

a) Material Coupling:

Conductivity $\underset{\sim}{k} = \underset{\sim}{k}(\underset{\sim}{\varepsilon}, T, \nabla\underset{\sim}{T})$ } from the principle of

Free energy $\Psi = \Psi(\underset{\sim}{\varepsilon}, T)$ } equipresence of state variables

b) Physical Coupling: Presence of $\dot{\underset{\sim}{\varepsilon}}$ in equation (1).

There is very little experimental evidence indicating that the conductivity $\underset{\sim}{k}$ is a function of deformation; in most cases even the dependence on temperature gradients must be neglected due to lack of data. Normally, the free energy Ψ is a function of both, the deformation and the temperature, whereby the second term of the righthand side of equations (1) is solely dependent on temperature implying that material coupling is negligible if physical coupling does not occur. The importance of the physical coupling term involving $\dot{\underset{\sim}{\varepsilon}}$ becomes clearer if one considers an adiabatic process for which

$$\frac{\partial^2\Psi}{\partial\underset{\sim}{\varepsilon}\,\partial T}:\dot{\underset{\sim}{\varepsilon}} = -\frac{\partial^2\Psi}{\partial T^2}\dot{T} \qquad (2)$$

Equation (2) suggests that physical coupling disappears for quasistatic motions, where the body moves slowly through a sequence of equilibrium positions without exhibiting inertia effects. Vice versa for the gradual process of heat conduction, where temperatures vary slowly, the velocities remain so small that inertia effects can be neglected. From these observations it can be concluded that thermomechanical coupling should be considered in the case of e.g. thermoelasto dynamics, but not in the case of thermoelasto statics. For the solution of certain restricted classes of coupled thermoelastic field problems using the finite element method, the reader may consult for example references [3], [4] and [5].

Since the present investigation deals exclusively with the thermomechanical response analysis, the heat conduction analysis is summarized only briefly. Among the first presentations of the finite element discretisation of the uncoupled heat balance equation one should mention references [6, 7, 8, 9, 10], in which the latter three also include the transient case. The discretised form of the heat balance equation may be written in matrix notation as

$$\mathbf{C}\dot{\mathbf{T}} + \mathbf{K}\mathbf{T} = \mathbf{Q} \qquad (3)$$

$\mathbf{C}$ denotes the consistent heat capacity matrix, $\mathbf{K}$ the heat conductivity matrix and $\mathbf{Q}$ the thermal flux vector. This coupled set of first order differential equations is solved for the temperature distribution either by direct time integration or by spectral decomposition (mode superposition) similarly to procedures used for the dynamic response analysis. Explicit and implicit techniques can be applied for the solution of the parabolic problem. Normally only single step algorithms are feasible because of the excessive storage and stability requirements of multistep

---

* Invariant notation is used to formulate the equations of continuum mechanics. The symbols $\sim$, : , $\cdot$ denote vectorfields, tensor contraction and inner products.

techniques. The Wilson-Nickell algorithm [7], a mid-step algorithm similar to the Crank-Nicholson procedure, is utilized in the present investigation. Reference [10] gives a more detailed account of the finite element technique employed to solve the accompanying temperature problem.

III QUASISTATIC FINITE ELEMENT FORMULATION

In the context of non-isothermal thermomechanical problems there are two possibilities to describe the initial value problem, either by differential or by integral formulation. In extension of the standard incremental description this investigation is based on the rate (differential) formulation, as the thermomechanical constitutive relations are defined in the same form. The time dependence may not be omitted in this context, since the stress-strain relations contain, ingeneral, non-homogeneous expressions of stress- and strain-rates, e.g. for creep and relaxation.

1. Formulation of Initial Value Problem

The governing field equations can be separated into static and kinematic relations, which take in invariant notation the following form

Quasistatic Equilibrium :

$$\nabla \cdot \dot{\underset{\sim}{\sigma}} + \dot{\underset{\sim}{f}} = 0 \qquad (4)$$

prescribed

$$\dot{\underset{\sim}{\sigma}}^{t} = \dot{\underset{\sim}{\bar{\sigma}}} \qquad \underset{\sim}{n} \cdot \dot{\underset{\sim}{\sigma}} = \dot{\underset{\sim}{\bar{p}}}$$

Kinematic Relations :

$$\dot{\underset{\sim}{\varepsilon}} = \tfrac{1}{2} \left(\nabla \dot{\underset{\sim}{u}} + \nabla \dot{\underset{\sim}{u}}^{t} \right) \qquad (5)$$

prescribed

$$\dot{\underset{\sim}{u}} = \dot{\underset{\sim}{\bar{u}}}$$

An appropriate generalisation of the principle of virtual work provides an equivalent statement to equations (4) and (5). Expressing the virtual work in virtual velocities and equating it to zero one obtains the following relation

$$\int_V \delta \dot{\underset{\sim}{\varepsilon}}^{t} \cdot \dot{\underset{\sim}{\sigma}} \, dV = \int_V \delta \dot{\underset{\sim}{u}}^{t} \cdot \dot{\underset{\sim}{f}} \, dV + \int_S \delta \dot{\underset{\sim}{u}}^{t} \cdot \dot{\underset{\sim}{p}} \, dS \qquad (6)$$

Equation (6) may be interpreted in the following way: If the virtual work is zero for any arbitrary infinitesimal virtual velocity field satisfying the kinematic relations (5), the mechanical system is in quasistatic equilibrium. Hence, the principle can be used to construct the quasi-static relations (4), if stress-strain rate relations are introduced. This procedure forms the basis for the finite element approximation method, using displacement models. For problems where the virtual work expression remains homogeneous in the rate terms the time derivatives can be omitted yielding the well-known incremental formulation for the solution of non-linear problems.

It should be emphasized that the principle of virtual work can be readily applied to non-conservative loading and that the constitutive relations need not be derivable from potential functions. The generalisation of the virtual work formulation is hence more flexible than alternative descriptions of the initial value problem using extensions of stationary variational principles.

For the complete formulation of the quasistatic problem equations (4) and (5) need to be supplemented by appropriate initial conditions at time $t = 0$

Initial static conditions:

$$\left.\begin{aligned} \mathbf{n}\cdot\dot{\boldsymbol{\sigma}} &= \dot{\mathbf{p}}_o \\ \mathbf{n}\cdot\boldsymbol{\sigma} &= \mathbf{p}_o \end{aligned}\right\} \text{"natural conditions"} \qquad (7)$$

Initial kinematic conditions:

$$\begin{aligned} \dot{\mathbf{u}} &= \dot{\mathbf{u}}_o \\ \mathbf{u} &= \mathbf{u}_o \end{aligned} \qquad (8)$$

2. Finite Element Discretisation

The virtual work equation (6) is now approximated with the help of finite element displacement models to construct a discrete form of the quasistatic relations. The finite element approximations may be written in matrix notation* as follows:

Velocity field $$\dot{\mathbf{u}} = \Phi_u \dot{\varrho}_u \qquad (9)$$

Initial strain-rate field $$\dot{\eta} = \Phi_\eta \dot{\varrho}_\eta \qquad (10)$$

Initial stress-rate field $$\dot{\tau} = \Phi_\tau \dot{\varrho}_\tau \qquad (11)$$

Total strain-rate field $$\dot{\gamma} = \dot{e} + \dot{\eta} = \nabla\Phi_u \dot{\varrho}_u \qquad (12)$$

Effective stress-rate field

$$\dot{\sigma} = E\dot{e} = E(\dot{\gamma} - \dot{\eta}) = E\dot{\gamma} + \dot{\tau}$$

$$= E(\nabla\Phi_u \dot{\varrho}_u - \Phi_\eta \dot{\varrho}_\eta) \qquad (13)$$

$$= E\nabla\Phi_u \dot{\varrho}_u + \Phi_\tau \dot{\varrho}_\tau \qquad (14)$$

The displacement interpolation Φ_u forms the basis for the spatial approximation of the displacement field $\mathbf{u}$ with $\dot{\varrho}_u$ denoting the column vector of nodal velocity values. The spatial distribution of elastically suppressed initial strains or equivalent initial stresses are described by the interpolation function Φ_η and Φ_τ. From a comparison of equations (13) and (14) it should be noted that both initial load approximations must satisfy the relation

$$\Phi_\tau \dot{\varrho}_\tau = -E\,\Phi_\eta \dot{\varrho}_\eta \qquad (15)$$

The initial stress and strain concept was introduced already in 1954 by the senior author [11] within the context of matrix (finite element) analysis of structures. It provides an ideal mechanism to account for elastically suppressed deformations arising from environmental conditions, such as temperature, moisture, irradiation, as well as mechanical conditions, such as non-linearity, e.g. plasticity and creep. Within the frame of the generalised principle of virtual work all initial loads have to be considered prescribed with the exception of the instantaneous plastic strains or stresses which should be derived from the total strain-rate field $\dot{\gamma}$.

Substituting the field approximations into the virtual work equation one obtains the well-known quasistatic equilibrium equations for a typical finite element

$$k\,\dot{\varrho}_u = \dot{P} + \dot{J} \qquad (16)$$

---

* Bold founts denote matrices and vectors

The element quantities are defined as follows

Stiffness
$$k = \int_V \nabla \Phi_u^t \, E \, \nabla \Phi_u \, dV \tag{17}$$

Nodal forces
$$\dot{P} = \int_V \Phi_u^t \, \Phi_f \, dV \, \dot{\varrho}_f + \int_S \Phi_u^t \, \Phi_p \, dS \, \dot{\varrho}_p \tag{18}$$

Initial loads
$$\dot{J} = \int_V \nabla \Phi_u^t \, E \, \Phi_\eta \, dV \, \dot{\varrho}_\eta$$
$$= -\int_V \nabla \Phi_u^t \, \Phi_\tau \, dV \, \dot{\varrho}_\tau \tag{19}$$

Subsequently, the individual element quantities are assembled with the help of the displacement method furnishing the desired quasistatic equilibrium equations of the structure

$$K \dot{r} = \dot{R} + \dot{R}_J \tag{20}$$

3. Certain Remarks on Finite Element Approximations

In the previous section it was mentioned that two types of initial stresses and strains should be distinguished, those whose spatial variation is prescribed e.g. due to given temperature distribution and those whose variation should be derived from the displacement approximation, e.g. in the case of plasticity. The first part of this section deals with the occurrence of residual stresses which arise in the case of certain finite element approximations although the continuum is stress-free. The second part is concerned with additional approximations involving higher order elements where the spatial distribution of plastic work is represented by various interpolation schemes, instead of being derived from the variation of the total strain field.

a) Representation of Linear Strain States

Using the compatibility equations of elasticity [1] it can be shown that linear strain distributions satisfying internal compatibility do not give rise to effective stresses within a three-dimensional continuum, if no constraints are enforced due to kinematic boundary conditions. Within the context of thermal problems this implies that no effective temperature stresses may occur for linearly varying temperature fields. Hence, for a finite element discretisation of the continuum the selected total strain variation γ should contain linear strain states within each element. From equation (13) the linearly varying temperature distribution is described by initial strains as follows

$$T = a + b x \quad \rightarrow \quad \eta_\Theta = \Phi_1 \alpha T$$

where a and b are scalars and Φ_1 denotes a linear interpolation scheme. If the effective stresses should remain zero

$$\sigma = E \left(\nabla \Phi_u \varrho_u - \Phi_1 \alpha T \right) = 0$$

hence

$$\nabla \Phi_u \supseteq \Phi_1 \tag{21}$$

Note, that equation (21) holds only symbolically, implying that the order of variation of the displacement gradients $\nabla \Phi_u$ should contain linear strain states. General finite element theory states that the finite element approximation must include rigid-body modes as well as constant strain states to ensure convergence in the energy sense (completeness requirement, see e.g. [12]). Equ. (21) represents a further restriction on the finite element approximation, if artificial residual stresses due to linear initial strains are to be avoided. Although

this requirement is not necessary for energy convergence, the exact reproduction of linear strain variation is a highly desirable feature for practical applications.

The question arises now about the additional restrictions on the finite element approximation, which are necessary to retain linear strain states. To simplify the algebra, only the u-displacement component is considered together with its variation in the x-direction. The other components of the vector field follow the same argument. It is obvious that an element contains linear strain states, if the approximated displacement field is able to vary with the square of the coordinates at any point of the element. In other words, if the nodal displacements are defined by

$$\varrho_i = a x_i^2 \qquad \text{where } a \text{ is a scalar,} \tag{22}$$

then $u = a x^2$ should be satisfied everywhere. Substituting these nodal displacements into the finite element approximation of equation (9), one obtains

$$u = \Phi_{ui} \varrho_i = \Phi_{ui} a x_i^2 = a \Phi_{ui} x_i^2 \tag{23}$$

If the element geometry is described by the interpolation scheme Φ_x, then

$$x = \Phi_{xj} x_j \tag{24}$$

and

$$u = a x^2 = a \left(\Phi_{xj} x_j \right)^2 \tag{25}$$

The linear strain condition is satisfied if equations (23) and (25) yield identical results at every point of the element leading to the following condition

$$\Phi_{ui} x_i^2 \geq \left(\Phi_{xj} x_j \right)^2 \tag{26}$$

We recall that Φ_u^i denotes the approximation of the displacement field defined by i nodes, while Φ_x^j denotes the description of the element geometry which may be defined by j nodes. Condition (26) demonstrates clearly that in isoparametric elements where $\Phi_x = \Phi_u$ linear strain states are not contained.

Isoparametric elements: $\Phi_x = \Phi_u = \Phi$ with $i = j$ (27)

Linear strain condition: $\Phi_i x_i^2 \neq \left(\Phi_i x_i \right)^2$ (28)

Equality in equation (28) cannot be achieved due to the presence of the mixed terms on the right-hand side. The linear strain condition (26) suggests that subparametric elements where $\Phi_u \supset \Phi_x$ can reproduce linear strain states if the order of the displacement approximation contains the square of the geometric approximation. For example, consider a linear interpolation scheme for the geometry and a quadratic one for the displacements

with $\Phi_x = \Phi_1$ and $\Phi_u = \Phi_2$ (29)

One may expect satisfaction of the linear strain condition if

$$\Phi_{2i} x_i^2 \geq \left(\Phi_{1j} x_j \right)^2 \tag{30}$$

Since algebra is extremely tedious, it is considered preferable to investigate the linear strain condition for a number of well established displacement models using numerical experiments. For simplicity, a square membrane subjected to linear temperature variation is chosen to assess the appearance and order of magnitude of residual stresses. Fig. 1 illustrates the geometrical and material properties of the problem together with the boundary conditions and temperature loading. The plane membrane is discretised by 25 nodes, each with two in-plane degrees of freedom, using Lagrangian interpolation. The effect of two parameters is investigated, the order of geometric approximation and the order of displacement approximation.

Fig. 2 illustrates the finite element lay-out of Phase I, where only square elements or isosceles triangles are used. This discretisation implies that $\Phi_x = \Phi_0$, which is synonymous to a constant "Jacobian". It also shows the element types used for the analysis, the linear displacement models like TRIM3 and QUAM4 with $\Phi_u = \Phi_1$, and the quadratic displacement models like TRIM6, [14], QUAM8 [40], [41] and QUAM9 [42], having $\Phi_u = \Phi_2$ with the exception of QUAM8 where $\Phi_u \subset \Phi_2$.

Fig. 3 illustrates the finite element lay-out of Phase II, where general quadrilateral and triangular elements are used. This discretisation implies that $\Phi_x = \Phi_1$, which is synonymous to a linear variation of the Jacobian.

Finally, Fig. 4 shows the curvilinear finite element lay-out of Phase III, where isoparametric quadrilateral and triangular elements are used [42], [43]. This discretisation implies that $\Phi_x = \Phi_2$, which is synonymous to a quadratic variation of the Jacobian. The associated curved elements are denoted by QUAMC9 and TRIMC6.

The results of this investigation are summarised in Table 1, where values for the residual stresses are given which arise solely from the finite element approximation. The mean square root of all nodal octaheder normal stresses and shear stresses are presented in percent of the initial thermal stresses after averaging first the nodal values.

$E = 1.0$ $\nu = 0.0$ $\alpha = 1.0$ $h = 1.0$		TRIM3 $\Phi_u = \Phi_1$	QUAM4 $\Phi_u = \Phi_1$	TRIM6 $\Phi_u = \Phi_2$	QUAM8 $\Phi_u = \Phi_2$	QUAM9 $\Phi_u = \Phi_2$	TRIMC6 $\Phi_u = \Phi_2$	QUAMC9 $\Phi_u = \Phi_2$
Phase I $\Phi_x = \Phi_0$	$\bar{\sigma}_0$	1.85	3.88	0	0	0		
	$\bar{\tau}_0$	1.88	5.79	0	0	0		
Phase II $\Phi_x = \Phi_1$	$\bar{\sigma}_0$	2.15	3.34	0	0.30	0	-	
	$\bar{\tau}_0$	2.37	4.86	0	0.54	0		
Phase III $\Phi_x = \Phi_2$	$\bar{\sigma}_0$	-		-			12.50	30.67
	$\bar{\tau}_0$						14.17	34.34

Table 1 Residual Stresses in Percent of Prescribed Temperature Stresses

The results for TRIM6 and QUAM9 clearly confirm that elements with a quadratic or biquadratic displacement field and a linear or bilinear geometric description do contain exactly the linear strain states, which must be expected from equation (30). All other elements give rise to residual stresses due to linear variation of initial thermal strains. This has to be expected for the constant strain triangle TRIM3 and the associated quadrilateral QUAM4, since they simply cannot reproduce linear strain states due to the low order of the displacement approximation. The residual stresses from QUAM4 are consistently worse than those of TRIM3, because simple averaging of the linear initial strains is only possible for the TRIM3. It is interesting to note that the element QUAM8 does not contain the linear strain states for a linearly varying Jacobian, since it is based on an incomplete quadratic displacement interpolation. Furthermore, the isoparametric elements TRIMC6 and QUAMC9 create considerable residual stresses due to their "geometric distortion". It should be remarked that a more severe distortion of the elements gives rise to even larger residual stresses, an eccentric positioning of the midside nodes being particularly harmful to the quality of stresses.

The variation of some residual stresses is illustrated in form of contourline plots on Figs. 5 to 8. There the distribution of octaheder shear,which is normalised in respect to the initial thermal stress, is shown for Phase II and III using the isoparametric elements TRIM3, QUAM4, TRIMC6 and QUAMC9. It should be mentioned that some resulting stress components are of an order higher than the octaheder stresses which are proportional to the first and second stress invariant. Moreover, the contour line plots are based on average nodal values which are used as base points for a linear interpolation scheme; hence they can not reflect the staggering discontinuities of stress components which occur e.g. at the center node raising the old question of an appropriate stress evaluation. When using average nodal values, it is quite clear that the amount of data handling reduces considerably for nodes on the element boundary versus internal element nodes. Furthermore, the user is mainly interested in the values at the corner nodes which are easily identified and which also allow a very useful check of the accuracy of the finite element idealisation for nodes where the "natural" boundary conditions should be satisfied. On the other hand it is interesting to note that the stress distribution in the interior of an element seems less affected by the geometric distortion discussed above. This is particularly true in the vicinity of the element centroid suggesting the use of centroidal stress points.

Since this investigation is rather preliminary in nature, only a few observations could be made. In conclusion one can say that the subparametric elements TRIM6 and QUAM9 are preferable to other elements as they do not give rise to artificial residual stresses in case of linear initial stress or strain problems. Caution should be exercised in the case that distorted elements are used to describe the geometry of the structure. Especially the eccentricity of the midside nodes impairs the resulting stress distribution which may offset the improvement gained by a more accurate geometric representation of the real structure.

b) Plastic Work Approximation in Higher Order Elements

For finite element displacement models the kinematic assumptions form the basis for the description of internal energy within each element. Given a unique relationship between stresses and total strains the spatial variation of internal energy is completely determined by the distribution of total strains. It is obvious that non-linear constitutive laws create additional problems for representing stresses or initial strains in higher order elements, in which the total strain distribution varies inside the element. In what follows, certain questions of approximation are dealt with in connection with the tangential stiffness method as applied to the elasto-plastic analysis using higher order elements.

The incremental elasto-plastic stress-strain relation is described by

$$\dot{\boldsymbol{\sigma}} = \mathbf{F}\,\dot{\boldsymbol{\gamma}} \tag{31}$$

For duality of the transformation laws the states of stress and strain are defined for the case of plane stress by

$$\boldsymbol{\sigma} = \{\sigma_{xx}\ \sigma_{yy}\ \sqrt{2}\,\sigma_{xy}\} \qquad \boldsymbol{\gamma} = \{\gamma_{xx}\ \gamma_{yy}\ \tfrac{1}{\sqrt{2}}\gamma_{xy}\} \tag{32}$$

For isotropic materials and the von Mises yield criterion with the Prandtl-Reuss flow rule the elasto-plastic material law can be written as follows [38]

$$\mathbf{F} = \left(\mathbf{I}_3 - \frac{1}{\xi + \mathbf{s}^t\mathbf{E}\,\mathbf{s}}\,\mathbf{E}\,\mathbf{s}\mathbf{s}^t\right)\mathbf{E} \tag{33}$$

with

$$\mathbf{s} = \frac{3}{2\,\bar{\sigma}}\,\boldsymbol{\sigma}_D \qquad \bar{\sigma}^2 = \tfrac{3}{2}\,\boldsymbol{\sigma}_D^t\boldsymbol{\sigma} \tag{34}$$

where the subscript D denotes deviatoric components and where ξ, the plastic strain-hardening parameter, is obtained from uniaxial data

$$\dot{\bar{\eta}}_P = \frac{1}{\xi}\,\dot{\bar{\sigma}} \tag{35}$$

The linear elastic material law reads for the isotropic case

$$\mathbf{E} = 2G\left(\mathbf{I}_3 + \frac{\nu}{1-\nu}\,\mathbf{e}_{2,1}\mathbf{e}_{2,1}^t\right) \tag{36}$$

with

$$\mathbf{e}_{2,1} = \{1\ 1\ 0\} \tag{37}$$

A more detailed derivation of the elasto-plastic relationships is given in Section IV for tri-axial conditions.

The elasto-plastic element stiffness is obtained simply by replacing the linear elastic material law in the expression of the strain energy density by its elasto-plastic extension, such that

$$\mathbf{k}_p = \int_V \boldsymbol{\Phi}_\gamma^t\,\mathbf{F}\,\boldsymbol{\Phi}_\gamma\,dV \tag{38}$$

Note, that in this case the elasto-plastic stiffness refers to the straining modes $\boldsymbol{\varphi}_\gamma$, which are identical with the so-called natural deformation modes $\boldsymbol{\varphi}_N$ introduced in [13]. It is obvious that the integral in (38) has to be evaluated numerically even for simple element configurations.

The question arises now about the representation of the elasto-plastic material law for deviatoric stresses which vary within the element domain. Basically, there are two possible avenues for implementing the tangential stiffness formulation using higher order elements: The direct integration route involving the construction of the elasto-plastic material law (33) at every pivot point of the numerical integration scheme, and the interpolation of the nonlinear stress-strain law from a chosen set of base points which can be written as

$$F = \Phi_F \varrho_F \tag{39}$$

Our main goal is now to obtain quantitative results for the effect of the different schemes when forming the elasto-plastic stiffness matrix. To this end, the spectrum of eigenvalues of the difference matrix between the reference and current stiffness provides a convenient norm to measure the difference of internal energy between two associated matrices. This method has proven useful in [45] to compare stiffness matrices of an element family having identical nodal configurations. The total internal energy rate of an elasto-plastic element is given by

$$\dot{U}_p = \dot{\varrho}_\gamma^t \, k_p \, \dot{\varrho}_\gamma \tag{40}$$

This increment of internal energy can be expressed in terms of the eigenvalues of k_p in the following form

$$x^t k_p x = \lambda I \tag{41}$$

where any set of nodal strain increments $\dot{\varrho}_\gamma$ can be represented as a linear combination of the set of eigenvectors x. The spectrum of eigenvalues of k represents a measure for the total internal energy rate of an element, hence this tool can also be utilized to determine the energy difference between a reference element and the element currently under investigation. It should be emphasized that only the eigenvalues of the difference matrix $k_r - k_c$ form a proper measure of this energy in contradistinction to the difference of eigenvalues of each individual stiffness matrix which in general do not correspond to the same eigenvectors. Thus

$$(\dot{U}_r - \dot{U}_c)_p = X^t (k_r - k_c)_p X = \Delta \tag{42}$$

X denotes the matrix of orthonormal eigenvectors of the difference matrix $k_r - k_c$ and Δ stands for a diagonal matrix containing all eigenvalues.

The associated spectral radius of the difference matrix forms a suitable norm to measure the "distance" between the reference stiffness and the current stiffness under investigation. The spread of eigenvalues indicates the variation of the difference between the two matrices for all possible deformation states, while the arithmetic mean yields a value illustrating the deviation of internal energy representation which can be expected in an average sense. Note that only positive or negative definite difference matrices permit a simple conclusion about the current stiffness being more flexible or more stiff than the reference stiffness.

In general the element stiffness is affected by two parameters, the material properties and the geometry. For the present considerations, attention is restricted to an equilateral linear strain triangle TRIM6, where the geometric effects are eliminated and where the total strain variation is defined by the linear interpolation scheme

$$\Phi_{\gamma} = \Phi_{1} \tag{43}$$

A representative choice for the "true" variation of the elasto-plastic material law forms the main difficulty in illustrating the evaluation of the elasto-plastic stiffness matrix using different interpolation and integration schemes. In order to avoid any bias in the representation of the material law, it should be assumed that the whole element domain plastifies instantaneously, while for simplicity the deviatoric stress components vary linearly over the element domain, as illustrated in Fig. 9. This stress assumption is valid for incipient plastic deformation only where no plastic deformation history yet distorts the linear stress distribution in the element. It should be mentioned that this condition cannot be realized since for a linear stress distribution the equivalent stresses form a second order surface over the element domain for which

$$\bar{\sigma}^2 = \frac{2}{3}\,\boldsymbol{\sigma}_D^t\boldsymbol{\sigma} \neq \text{const} \tag{44}$$

To achieve instantaneous plastification of the whole element it has to be further assumed, either that the yield limit varies over the element domain according to the shape of the equivalent stress or that the plastic deformation history is followed only at the point where $\bar{\sigma} = \bar{\sigma}_{min}$. We adopt below the second line of thought with the following material properties assuming that constant strain hardening, as illustrated in Fig. 10, prevails throughout the element and that the plastic deformation histories of other points need not be considered.

In the example, the following data were assumed:

Yield Stress:	$\bar{\sigma}_y$	= 19.4	kp/mm^2
Strain Hardening:	ξ	= 0.3	kp/mm^2
Elastic Modulus:	E	= 21000	kp/mm^2
Poisson's Ratio:	ν	= 0.3	

The elasto-plastic stiffness matrix calculated with a 30 x 30 Gaussian quadrature rule is regarded as the "exact" reference stiffness for the subsequent investigation of various matrices. This implies that the elasto-plastic material law is evaluated at the 900 pivot points for the assumed distribution of deviatoric stresses and material constants. Subsequently, elasto-plastic stiffness matrices are constructed either by direct integration involving the evaluation of the elasto-plastic material law from the governing stress distribution of the pivot point considered, or by interpolation from a chosen set of base points. We then compare these elasto-plastic stiffness matrices with the reference matrix using the concept of eigenvalues of each difference matrix mentioned above.

The following numerical integration schemes are selected for comparison: 1 point, 2 point, 3 point, 4 point, 6 point and 12 point Gaussian quadrature rules. The range of eigenvalues is illustrated in Fig. 11 for each stiffness difference matrix.

$$X^t (k_{3o} - k_{int})_p X = \Delta \qquad (46)$$

Order of Integration: int. = 1, 2, 3, 4, 6, 12

The results are plotted in terms of the numbers of material data points which coincide in this case with the number of pivot points of the quadrature rule.

This presentation is particularly useful since it illustrates the deviation of the elasto-plastic stiffness from the reference stiffness as function of the amount of the necessary data handling.

Alternatively to the direct integration route, five Lagrangian interpolation schemes shown in Fig. 12 are selected to approximate the distribution of the elasto-plastic material law over the element domain. Besides the constant, linear, quadratic and cubic interpolations, a piecewise linear interpolation scheme over triangular subregions, as proposed in [44], is chosen to represent the material law. The elasto-plastic stiffness is evaluated using a 30 x 30 Gaussian quadrature rule, but in contradistinction to the reference stiffness, only the base points of the interpolation scheme now form material data points. The range of eigenvalues is illustrated in Fig. 13 for each stiffness difference matrix. Again the results are presented in terms of the number of material data points involved in different interpolation schemes to allow a direct comparison with the range of eigenvalues of the direct integration methods. Note that only linear interpolation preserves the positive definiteness of the material law within the element domain. E.g. Fig. 14 illustrates the non-positive definite material regions which are artificially introduced by cubic interpolation even though the material law at the base points is positive definite; therefore, Fig. 13 shows two different results for the cubic interpolation as the elasto-plastic stiffness can be evaluated either neglecting or considering the type of material law encountered at each pivot point, the second of which may lead to a non-positive definite stiffness matrix. From these observations it is quite clear that higher order interpolation of the material law should be avoided altogether, since it changes the character of the material law instead of improving its representation.

Comparing Fig. 11 and Fig. 13 one can see the distortion of the "exact" elasto-plastic stiffness due to the direct integration method and the interpolation method for the same number of material data points involved. It seems that the interpolation schemes yield consistently worse results than the corresponding direct integration schemes except for the linear interpolation over triangular subregions. This method of material representation offers a slight advantage considering that the total amount of data handling reduces sharply for the element assembly, where the valency of the edge nodes varies between 2 and 6 in contradistinction to the single valency for the interior data points of the direct integration method.

Finally, it should be mentioned that this element investigation using the eigenvalue technique of stiffness difference matrices is preliminary in nature and should be accompanied by similar numerical experiments on the structural level to verify quantitatively the qualitative element results.

IV CONSTITUTIVE LAWS

In this section a number of engineering theories are considered to describe the material behavior in thermal environments. Emphasis is placed on the time rate formulation of constitutive relations fitting the scope of the quasistatic formulation. The following discussion is restricted to thermomechanically simple materials where the response at a given instant of time is determined by the histories of deformation and temperature.

A realistic material description should consider temperature dependent material properties leading in general to stress-strain relations non-linear in the temperature. Under non-isothermal conditions this temperature dependency gives rise to time variable material behaviour. The subtle point of the material ageing will be treated in the following section on thermoelasticity, where two fundamentally different material descriptions are reviewed and applied to solve a thermoelastic problem. Subsequently, the well-known elasto-plastic stress-strain relations are extended to include temperature effects including temperature dependent yielding. It will be further shown how the engineering theory of creep may be simply incorporated in the thermoelasto-plastic material law to account for viscous effects. This general constitutive law is then applied to the solution of a realistic engineering problem.

It should be emphasized that the virtual work formulation in terms of the rates permits the incorporation of very general constitutive relations as long as they define the instantaneous material response as function of deformation and temperature history. For this direct route there is no need to claim the existence of potentials from which the stress-strain relations may be derived.

1. Thermoelasticity

As introduction, the linear stress-strain relations are briefly reviewed for isothermal conditions. The three-dimensional cartesian form of Hooke's law may be stated in matrix notation as follows

$$\boldsymbol{\sigma} = \mathbf{E}\,\boldsymbol{\varepsilon} \tag{47}$$

where $\boldsymbol{\sigma}$, the stress vector, having six components, is related to the corresponding strain vector $\boldsymbol{\varepsilon}$ by the linearly elastic material law $\mathbf{E}$ involving 21 constants in case of general anisotropy. The thermal expansion due to a temperature change may be interpreted as mapping of the neighbourhood of a material point into a new configuration assuming all mechanical constraints can be temporarily neglected. Although the stress free thermal expansion may physically not be possible, this new configuration can be thought of as a reference state from which effective, stress producing, deformation is measured. Assuming that the changes of temperature remain small in regard to the reference temperature T_o, the thermal deformation may be described by the following expression which is linear in temperature

$$\boldsymbol{\eta}_\Theta = \boldsymbol{\alpha}\,(T - T_o) = \boldsymbol{\alpha}\,\Theta \tag{48}$$

where for the isotropic case the vector of coefficients of thermal expansion degenerates to

$$\boldsymbol{\alpha} = \alpha\,\mathbf{e}_{3,3} \qquad \text{with} \qquad \mathbf{e}_{3,3} = \{\,1\ 1\ 1\ 0\ 0\ 0\,\} \tag{49}$$

The coefficients of thermal expansion are independent of temperature for changes of temperature $\Theta = T - T_o$ less than 40°C [2]. This linear form of the fundamental decomposition for thermomechanical deformation forms the basis of the well-known generalisation of Hooke's law also named after Duhamel-Neumann

$$\gamma = \varepsilon + \eta_\theta = \varepsilon + \alpha\,\theta = E^{-1}\sigma + \alpha\,\theta \qquad (50)$$

or

$$\sigma = E\,(\gamma - \alpha\,\theta) = E\,\gamma + \theta\beta = E\,\gamma + \tau_\theta \qquad (51)$$

where the initial temperature stresses are defined by

$$\tau_\theta = \theta\,\beta \qquad \text{and} \qquad \beta = -E\,\alpha \qquad (52)$$

Under the assumption of weak coupling the distribution of transient temperatures can be considered prescribed at each instant of time as

$$T = T(t) \qquad \text{and} \qquad \theta = \theta(t) \qquad (53)$$

Hence, for temperature dependent material properties the thermal stress analysis involves ageing material properties or in other words a time variable system since

$$\begin{aligned} E\,(T) &= E\,(t) \\ \beta\,(T) &= \beta\,(t) \end{aligned} \qquad (54)$$

For non-isothermal conditions there are two possibilities to describe the elastic material response, which differ fundamentally if temperature dependent material properties are considered: the classical hyperelastic formulation and the hypoelastic characterization which are summarized below [1].

a) Hyperelastic Formulation

In the classical sense an elastic material possesses a natural state in thermodynamic equilibrium at which $\sigma = 0$ and $T = T_0$ exhibiting a unique one to one correspondence between stress and strain in an appropriate neighbourhood of this reference state. The material is characterized by its return to the natural state after removal of loading, or in other words the domain of the hyperelastic response functional contains no history effects. From this postulate of elastic material behaviour (51) can be generalized, leading to the following "integral" relation

$$\sigma = E\,(t)\,\gamma + \int_{T_0}^{T} \beta(\tau)\,d\tau \qquad (55)$$

Equation (55) describes essentially an ageing viscoelastic material with infinitely short memory. It should be emphasized that this characterization is restricted by the definition of an appropriate neighbourhood from the natural state. Formal differentiation in time furnishes the equivalent rate formulation exhibiting non-homogeneous terms in γ and θ

$$\dot{\sigma} = E\,(t)\,\dot{\gamma} + \beta\,(t)\,\dot{\theta} + \dot{E}\,(t)\,\gamma + \dot{\beta}\,(t)\,\theta \qquad (56)$$

This equation represents a total differential ensuring reversibility and path-independency of the thermoelastic process. These properties are intrinsic prerequisites for the existence of a thermoelastic potential from which hyperelastic stress-strain relations are usually derived.

It should be noted that due to the temperature dependence of E and β equation (56) is basically non-linear in temperature. In spite of this non-linearity there is no need to pursue an incremental approach for the thermal stress analysis. Since the temperatures are prescribed in the uncoupled problem the total stress relation of equation (55) can be used directly to determine the hyperelastic response at any instant of time. Note that in this case the material must possess a natural state to which it returns after unloading and that an appropriate neighbourhood is defined for the excursions from this reference state.

b) Hypoelastic Formulation

In contradistinction to the hyperelastic description, the hypoelastic characterization of an elastic solid is formulated without reference to a natural state, and expresses the components of stress rate as homogeneous linear functions of the components of the total strainrate and temperature rate

$$\dot{\sigma} = E(t)\,\dot{\gamma} + \beta(t)\,\dot{T} \tag{57}$$

This implies that this constitutive law involves in addition to the homogeneous state variables σ, γ and T only mechanical properties characterizing the instantaneous state of the solid. These time variable moduli are independent of the speed at which changes of the state variables are affected. Thus

$$\dot{E}(t) = \dot{\beta}(t) = 0 \tag{58}$$

An equivalent integral formulation may be obtained from the principle of superposition on the rate expressions $\dot{\sigma}$, $\dot{\gamma}$ and $\dot{T}$. The well-known step formulation for ageing hypoelastic materials yields the following total stress expression

$$\sigma(t) = \int_{t_0^-}^{t} E(\tau)\,\frac{d}{d\tau}\left\{\gamma(\tau) - \Theta(\tau)\right\} d\tau \tag{59}$$

After integration by parts the equivalent impulse formulation furnishes

$$\sigma(t) = E(t)\left\{\gamma(t) - \Theta(t)\right\} - \int_{t_0^+}^{t} \frac{dE(\tau)}{d\tau}\left\{\gamma(\tau) - \Theta(\tau)\right\} d\tau \tag{60}$$

where the pseudo temperature Θ is defined by

$$\Theta(t) = \int_{T_0}^{T} \alpha(\tau)\, d\tau \tag{61}$$

The integral formulations clearly show that the stress at time t is a function of the entire strain and temperature history, the functional being linear in strains, but non-linear in temperature, Hence, this characterization basically implies that the elastic solid exhibits path dependency and irreversibility due to ageing effects similar to viscous phenomena. It should be remarked that the theory of hypoelasticity forms the basis for the hereditary integral representation of viscoelastic behaviour.

A comparison between the impulse formulation of equation (60) and the hyperelastic stress-strain relation (55) indicates that both material characterizations of elastic bodies coincide for time-invariable systems. Of course, the same conclusion is reached from a comparison of the analogous rate formulations, equations (56) and (57) . It is obvious that, if attention is restricted to close neighbourhoods of the natural state, such that constant material properties prevail, then the hypoelastic formulation degenerates to the hyperelastic one.

c) Numerical Implementation

The finite element analysis of the transient thermoelastic problem reduces to a straight-forward application of the initial load concept, see equations (16) and (20).

The integral relationship of the hyperelastic formulation (55) yields for temperature dependent mechanical properties a time-variable set of equilibrium relations of the following form

$$K(t)\, r(t) = R(t) + R_\theta(t) \tag{62}$$

Note that the instantaneous stiffness $\mathbf{K}(t)$ as well as the initial loading due to temperatures $\mathbf{R}_\theta(t)$ can be evaluated directly for any stage of the prescribed transient thermal conditions. For temperature independent mechanical properties equation (62) reduces to a time-invariable system in which $\mathbf{K}(t)=\mathbf{K}$, such that transient temperature conditions involve solely the solution of a number of loading conditions.

The rate type relationship of the hypoelastic formulation (57) furnishes for temperature dependent material properties a time-variable set of incremental equilibrium relations of the following form

$$\mathbf{K}(t)\,\mathbf{r}_\Delta(t) = \mathbf{R}_\Delta(t) + \mathbf{R}_{\theta\Delta}(t) \tag{63}$$

It should be emphasized again that the hypoelastic solid requires an incremental strategy for the thermal stress analysis, since the whole temperature history needs to be considered. Therefore, this formulation is far more laborious than the total stress analysis for the numerical implementation of hyperelastic material behaviour. In case of temperature independent mechanical properties the incremental equilibrium equation degenerates to equation (62) with a time-invariable stiffness.

d) Example

In conclusion the transient thermoelastic stress distribution is determined for an "infinite" medium with a spherical cavity, the boundary of the cavity being subjected to the sudden temperature rise $\Theta_i = 600^\circ$ F. Both, constant and temperature dependent material properties are dealt with using a hyperelastic and a hypoelastic description of the elastic behaviour. This polarly symmetric problem is selected as theoretical solutions are available for comparison with the finite element results for the case of constant material properties [16] as well as for the case of temperature dependent properties [17].

For the finite element analysis the infinite medium is idealised by a finite cylinder with a radius ten times the radius of the inner cavity and a height equal to the diameter of the cylinder. Because of symmetry only the upper half of the cylinder needs to be analysed. Both, the transient heat conduction analysis as well as the thermoelastic stress analysis is carried out using the same finite element mesh lay-out which is illustrated in Fig. 16. 192 axisymmetric TRIAX 6 elements are used to discretize the cylindrical structure with the cavity involving 425 nodal points. The reader is referred to [15] for a description of the triangular ring element TRIAX 6 having 6 nodes.

Two cases are treated, a medium with constant, temperature independent material properties and a temperature sensitive medium exhibiting more realistic material properties as occur in the case of SAE 1095 steel [18]. The temperature dependency of the elastic constants is described by

$$\begin{aligned}
&\text{Shear modulus} && G = 11.55 \times 10^6 \left(1 - 0.3463 \times 10^{-6}\,\Theta^2\right)\\
&\text{Poisson's ratio} && \nu = 0.345 + 0.7 \times 10^{-2} \left(\Theta - 565\right)^{1/3}\\
&\text{Thermal expansion} && \alpha = 0.65 \times 10^{-5} \left(1 + 0.9231 \times 10^{-3}\,\Theta\right)
\end{aligned} \tag{64}$$

Fig. 17 illustrates the variation of the elastic properties with temperature. For the finite element solution of the heat conduction problem the thermal diffusivity $k/\rho c$ is assumed to remain constant. The boundary conditions of the thermal problem consist only of the prescribed temperatures $\theta_i = 600^\circ$ F at the inner surface of the cavity and $\theta_s = 0^\circ$ F on the outside surface.

In order to simplify the comparison with the theoretical solution the following non-dimensional quantities are introduced

Time	$\tau = \frac{1}{a^2} \frac{k}{\rho c} t$	
Temperature	$\theta^* = \theta/\theta_i$	
Radial Displacement	$u_r^* = \frac{1-\nu}{1+\nu} \frac{1}{\alpha_o \theta_i a} u_r$	(65)
Radial Stress	$\sigma_r^* = \frac{1-\nu}{2(1+\nu)G} \frac{1}{\alpha_o \theta_i} \sigma_r$	
Hoop Stress	$\sigma_t^* = \frac{1-\nu}{2(1+\nu)G_o} \frac{1}{\alpha_o \theta_i} \sigma_t$	

To define the geometry of the problem, the radius of the spherical cavity is taken as $a = 1.0$ and the thermal diffusivity is assumed to be $k/\rho c = 1.0$. Since the theoretical solutions are based on the polarly symmetric treatment of the infinite medium, the results of the problem are only presented at various radial distances of the midsection through the cavity.

Fig. 18 illustrates the radial distribution of the transient temperatures $\theta^* = \theta/\theta_i$ after the sudden temperature rise $\theta_i = 600^\circ$ F at the cavity. The results of the theoretical heat conduction analysis for the infinite medium agree very well with those of the finite element solution for the cylinder. In the vicinity of the spherical cavity there is virtually no difference between both results. The time integration of the heat balance equation was carried out with variable time steps ranging from $\tau = 1/32$ to $\tau = 4$.

Two parameters are investigated by means of the following transient elastic stress analysis, the influence of temperature dependent material properties and the type of elastic formulation.

In Fig. 19, 20 and 21 displacements and stresses are compared in a temperature-sensitive and insensitive medium at different times τ after the temperature rise at the cavity. In the case of temperature-independent material properties, the finite element results for the cylinder are shown in addition to the theoretical solution for the infinite medium presented in [16]. The finite element results for the temperature-sensitive medium are obtained using the hyperelastic formulation; this means that at every instant of time the tangential stiffness has to be determined from the temperature dependent material properties of Fig. 17. It should be mentioned that a linear interpolation scheme is used to describe the variation of the elastic moduli within each TRIAX 6 element. Fig. 19 illustrates the radial distribution of displacements at various times τ. Note, that the displacements at the spherical cavity remain zero irrespective of the temperature rise at the cavity. For the temperature-insensitive properties there is very little difference between the analytic and the finite element solutions; these results deviate considerably from the temperature-sensitive results in regions of high temperature gradients. Fig. 20 presents an analogous illustration of transient radial stress components. Again, there is a significant difference between temperature-sensitive and insensitive properties in areas of

high temperature gradients. It may be of interest that the violation of the stress boundary condition $\sigma_r^* = 0$ at the cavity is very small in comparison to the large changes of σ_r^* in radial direction, hence the discretisation error seems negligible. In case of the long-term response of radial stresses the analytic solution deviates considerably from the finite element results in regions influenced by the different boundary conditions. Fig. 21 illustrates the distribution of tangential stresses at various times. There is hardly any noticeable difference between the two finite element solutions except right at the spherical cavity.

In Fig. 22, 23 and 24 transient displacements and stresses are compared in a temperature-sensitive medium, the response of which is described either by the hyperelastic or hypoelastic formulation. The finite element results are shown for the cylinder in addition to the corresponding theoretical solution of the infinite medium, presented in [17]. The finite element solutions are obtained using both, the total stress approach of the hyperelastic formulation for different instants of time, and the incremental stress approach of the hypoelastic description, proceeding through the temperature history. Poisson's ratio is assumed to remain constant at $\nu = 0.4$ since the theoretical results are based on that value. Fig. 22 illustrates the radial distribution of displacements at various times. Note that there is very little difference between the hyperelastic and hypoelastic results even in regions of high temperature gradients. The deviation of the analytic results can be explained due to the difference between the analytic and finite element temperature distributions, arising from the dependency of conductivity on the temperature in the former case [17]. The transient radial stress components, illustrated in Fig. 23, exhibit a more pronounced effect of the two possibilities to describe the elastic behaviour. Again, the long-term results of the analytic solution deviate considerably from the finite element results in regions influenced by the different boundary condition. Fig. 24 illustrates the distribution of tangential stresses at various times; these components are hardly affected by the two alternative formulations except near the spherical cavity.

In conclusion one may state that a realistic stress analysis should accommodate the temperature dependence of mechanical properties, since the assumption of temperature insensitivity underestimates considerably the structural response. The type of formulation to describe the elastic behaviour seems to have little influence onto the results. However, this statement applies only to the type of problem considered here, where the temperature sensitivity of the material properties remains relatively small. On the other hand, these quantitative results indicate that the hypoelastic formulation can be utilized if an incremental formulation is necessary, such as in plasticity and viscoelasticity. However, this costly method does not justify the expense, if applied to account for path dependency due to temperature dependent elastic properties in a transient thermal environment.

2. Thermoelastoplasticity and Creep

Following [19] and [21] the flow theory of plasticity is first reviewed in regard to non-isothermal conditions without taking recourse to thermodynamics. Subsequently, the general constitutive law is specialized to construct a set of thermo-elasto-plastic stress-strain relations which can be used to solve realistic engineering problems where high stresses of short duration occur under applied loads and temperatures. After presenting the time-independent stress-strain relation for plasticity, the formulation is extended to incorporate creep. Omitting history dependence of creep deformations, the phenomenological description of the engineering theory of creep is dealt with, which provides a simple means to account for viscous effects in metals. It is shown that the initial load techniques for the iterative solution of plasticity problems are

easily adjusted to incorporate creep. In conclusion an example is presented to illustrate the thermo-elasto- plastic and creep behaviour on a realistic engineering problem.

a) Thermo-elasto-plastic Formulation

Consider an elasto-plastic workhardening solid where for a given state infinitesimal changes of temperatures and stresses produce a unique infinitesimal change of elastic and plastic strains. It is assumed that the constitutive law is homogeneous of order one involving only the time rates $\dot{\sigma}$, $\dot{\eta}_p$ and $\dot{T}$, while the material properties characterize the instantaneous state of the solid analogous to the hypoelastic formulation. An additional state variable need to be defined to describe the dissipation of mechanical energy via

$$k = \int_0^t \sigma^t \dot{\eta}_p \, dt \tag{66}$$

where k denotes the workhardening parameter as a non-decreasing function of time. It is further assumed that there exists a function of the state variables $f(\sigma, \eta_p, T, k)$ which describes initial and subsequent yield surfaces for all plastic states. The time rate of the loading function f is utilized to define loading between two plastic states f and $f+df$, where

$$\dot{f} = \frac{\partial f}{\partial \sigma} \dot{\sigma} + \frac{\partial f}{\partial \eta_p} \dot{\eta}_p + \frac{\partial f}{\partial T} \dot{T} + \frac{\partial f}{\partial k} \dot{k} \tag{67}$$

The state of loading is defined by $f=0$.

and
$$\frac{\partial f}{\partial \sigma} \dot{\sigma} + \frac{\partial f}{\partial T} \dot{T} \begin{cases} < 0 & \text{Unloading} \\ = 0 & \text{Neutral Loading} \\ > 0 & \text{Plastic Loading} \end{cases} \tag{68}$$

The "normality condition", which follows from Drucker's stability postulate for inelastic materials [20], forms the basis of the associated flow rule

$$\dot{\eta}_p = \lambda \frac{\partial f}{\partial \sigma^t} \tag{69}$$

The positive scalar λ can be evaluated from Prager's consistency condition $\dot{f} = 0$

$$\lambda = - \frac{\left(\frac{\partial f}{\partial \sigma} \dot{\sigma} + \frac{\partial f}{\partial T} \dot{T} \right)}{\left(\frac{\partial f}{\partial \eta_p} + \frac{\partial f}{\partial k} \sigma^t \right) \frac{\partial f}{\partial \sigma^t}} \tag{70}$$

The generality of this formulation leaves ample room for experimental evidence which can be described by a variety of yield conditions and flow rules.

To be specific, the following discussion is concerned with the extension of the von Mises yield condition and the Prandtl-Reuss flow rule to non-isothermal conditions with temperature dependent hardening in extension of the formulation presented in [38]. For cyclic loading conditions, Prager's method of kinematic hardening or Ziegler's modification of this theory could be easily incorporated to account for the Bauschinger effect. Furthermore, in case of non-metallic materials the yield condition and flow rule could be adjusted to include the effects of hydrostatic pressure similar to Drucker's formulation for materials with internal friction and cohesion.

The formulation below is restricted to isotropic conditions where

$$E = 2G \left(I + \frac{\nu}{1-2\nu} e_{s,3} e_{s,3}^t \right) \tag{71}$$

For duality of stress and strain transformations the corresponding stress and strain vectors are defined as follows

$$\boldsymbol{\sigma} = \{ \sigma_{xx} \quad \sigma_{yy} \quad \sigma_{zz} \quad \sqrt{2}\,\sigma_{xy} \quad \sqrt{2}\,\sigma_{yz} \quad \sqrt{2}\,\sigma_{zx} \}$$
$$\boldsymbol{\gamma} = \{ \gamma_{xx} \quad \gamma_{yy} \quad \gamma_{zz} \quad \tfrac{1}{\sqrt{2}}\gamma_{xy} \quad \tfrac{1}{\sqrt{2}}\gamma_{yz} \quad \tfrac{1}{\sqrt{2}}\gamma_{zx} \} \tag{72}$$

For thermo-elasto-plastic behaviour the total deformation can be decomposed into

$$\dot{\boldsymbol{\gamma}} = \dot{\boldsymbol{e}} + \dot{\boldsymbol{\eta}}_p + \boldsymbol{\alpha}\,\dot{T} \tag{73}$$

For metals experimental evidence indicates that the initial yield condition and plastic deformation are not affected by hydrostatic stress and that plastic deformation takes place without volume change. Therefore, it is convenient to decompose stress and strain into hydrostatic and deviatoric components

$$\boldsymbol{\sigma} = \boldsymbol{\sigma}_H + \boldsymbol{\sigma}_D \qquad \text{and} \qquad \boldsymbol{\gamma} = \boldsymbol{\gamma}_H + \boldsymbol{\gamma}_D \tag{74}$$

For isotropic materials the initial yield function may be expressed entirely in terms of the invariants of the deviatoric stresses. The most widely used yield function, also known under the name of von Mises, describes the incipience of plastic deformation by the second invariant

$$f = \tfrac{3}{2}\boldsymbol{\sigma}_D^t\,\boldsymbol{\sigma}_D - \bar{\sigma}^2 = 0 \quad \rightarrow \quad \bar{\sigma}^2 = \tfrac{3}{2}\boldsymbol{\sigma}_D^t\,\boldsymbol{\sigma}_D \tag{75}$$

This yield condition also provides a definition for the scalar function $\bar{\sigma}$, the so-called von Mises equivalent stress, in terms of the deviatoric stress components. The associated flow rule yields then an expression for the plastic strain increment in terms of deviatoric stresses and an unknown scalar function λ

$$\dot{\boldsymbol{\eta}}_p = \lambda\,\frac{\partial f}{\partial \boldsymbol{\sigma}^t} = 3\lambda\,\boldsymbol{\sigma}_D \tag{76}$$

This scalar λ can be determined either with laborious manipulations from equation (70) or directly from the workhardening expression

$$\dot{k} = \boldsymbol{\sigma}_D^t\,\dot{\boldsymbol{\eta}}_p = \bar{\sigma}\,\dot{\bar{\eta}}_p \quad \rightarrow \quad \dot{\bar{\eta}}_p^2 = \tfrac{2}{3}\,\dot{\boldsymbol{\eta}}_p^t\,\boldsymbol{\eta}_p \tag{77}$$

This definition of the equivalent strain $\dot{\bar{\eta}}_p$ ensures that the plastic work remains the same for uniaxial and multiaxial conditions. Substituting equation (76) into equation (77) one obtains readily

$$\lambda = \frac{1}{2\bar{\sigma}}\,\dot{\bar{\eta}}_p \tag{78}$$

Inserting λ into the flow rule (76) leads subsequently to the following expression for the plastic strain increment

$$\dot{\boldsymbol{\eta}}_p = \dot{\bar{\eta}}_p\,\boldsymbol{s} \qquad \text{with} \qquad \boldsymbol{s} = \frac{3}{2\bar{\sigma}}\,\boldsymbol{\sigma}_D \tag{79}$$

In thermal environments the equivalent plastic strain is a function of stress and temperature

$$\bar{\eta}_p = \bar{\eta}(\bar{\sigma}, T) \quad \rightarrow \quad \dot{\bar{\eta}}_p = \frac{1}{f}\,\dot{\bar{\sigma}} + g\,\dot{T} \tag{80}$$

with

$$f = \frac{\partial \bar{\sigma}}{\partial \bar{\eta}_p} \qquad \text{and} \qquad g = \frac{\partial \bar{\eta}_p}{\partial T} \tag{81}$$

The physical significance of the parameters ζ and φ is illustrated in Fig. 25. This formulation was first presented in connection with the elasto-plastic matrix displacement analysis in [32].

There are two possibilities to proceed from now on: The equivalent plastic strain-rate can be defined either in terms of the effective stress rate or directly in terms of the total strain rate, leading to the following initial load schemes.

"Initial Strain Approach" $\qquad \dot{\bar{\eta}}_p = \dot{\bar{\eta}}_p (\mathbf{s}^t \dot{\boldsymbol{\sigma}} , \dot{T})$

This formulation describes the equivalent plastic strain-rate in terms of the increment of the elastic energy of distortion

$$\dot{\bar{\eta}}_p = \frac{1}{\zeta} \dot{\bar{\sigma}} + \varphi \dot{T} = \frac{1}{\zeta} \mathbf{s}^t \dot{\boldsymbol{\sigma}} + \varphi \dot{T} \tag{82}$$

leading to the following form of the flow rule

$$\dot{\boldsymbol{\eta}}_p = \frac{1}{\zeta} \mathbf{s}\mathbf{s}^t \dot{\boldsymbol{\sigma}} + \varphi \mathbf{s} \dot{T} \tag{83}$$

The total deformation rate can now be expressed by

$$\dot{\boldsymbol{\gamma}} = \dot{\mathbf{e}} + \dot{\boldsymbol{\eta}}_p + \boldsymbol{\alpha} \dot{T} = \mathbf{E}^{-1} \dot{\boldsymbol{\sigma}} + \frac{1}{\zeta} \mathbf{s}\mathbf{s}^t \dot{\boldsymbol{\sigma}} + (\varphi \mathbf{s} + \boldsymbol{\alpha}) \dot{T} \tag{84}$$

Hence, the desired strain-stress-temperature rate relationship can be written as

$$\dot{\boldsymbol{\gamma}} = \mathbf{E}^{-1} \left(\mathbf{I} + \frac{2G}{\zeta} \mathbf{s}\mathbf{s}^t \right) \dot{\boldsymbol{\sigma}} + (\boldsymbol{\alpha} + \varphi \mathbf{s}) \dot{T} \tag{85}$$

Note the additional plastic loading term $\varphi \mathbf{s} \dot{T}$ arising from the temperature dependence of the hardening law, see equation (80).

"Initial Stress Approach" $\qquad \dot{\bar{\eta}}_p = \dot{\bar{\eta}}_p (\mathbf{s}^t \dot{\boldsymbol{\gamma}} , \dot{T})$

This formulation describes the equivalent plastic strain-rate in terms of the increment of the total energy of distortion

$$\begin{aligned} \dot{\bar{\eta}}_p &= \frac{1}{\zeta} \mathbf{s}^t \mathbf{E} \left(\dot{\boldsymbol{\gamma}} - \dot{\boldsymbol{\eta}}_p - \boldsymbol{\alpha} \dot{T} \right) + \varphi \dot{T} \\ &= \frac{2G}{\zeta + 3G} \mathbf{s}^t \dot{\boldsymbol{\gamma}} + \frac{\zeta}{\zeta + 3G} \varphi \dot{T} \end{aligned} \tag{86}$$

leading to the following form of the flow rule

$$\dot{\boldsymbol{\eta}}_p = \frac{2G}{\zeta + 3G} \mathbf{s}\mathbf{s}^t \dot{\boldsymbol{\gamma}} + \frac{\zeta}{\zeta + 3G} \varphi \mathbf{s} \dot{T} \tag{87}$$

This forms the basis of the desired thermo-elasto-plastic stress-strain-temperature rate law, where the effective stress rate is defined by

$$\dot{\bar{\sigma}} = \mathbf{E} \dot{\mathbf{e}} = \mathbf{E} \left(\dot{\boldsymbol{\gamma}} - \dot{\boldsymbol{\eta}}_p - \boldsymbol{\alpha} \dot{T} \right) \tag{88}$$

$$\dot{\bar{\sigma}} = \mathbf{F} \dot{\boldsymbol{\gamma}} + \mathbf{G} \dot{T} \tag{89}$$

The "tangential" thermo-elasto-plastic material behaviour is described by $\mathbf{F}$ and $\mathbf{G}$, where

$$F = E\left(I - \frac{2G}{\xi + 3G}\, ss^t\right) \tag{90}$$

and

$$G = -E\left(\alpha + \frac{\xi}{\xi + 3G}\, \varphi s\right) \tag{91}$$

This thermo-elasto-plastic constitutive law furnishes the desired linear relationship between stress-, total strain- and temperature rates, which is strictly valid only in the differential sense.

It should be noted that the first terms on the right hand sides of equation (90) and (91) represent the linear elastic portion of the constitutive law and that the second terms constitute their corrections due to plasticity. It is easily verified that the tangential material law in equation (90) is the inverse of the first term on the right-hand side of the total strain rate relationship, equation (85).

b) Extension to Include Thermal Creep

The following discussion is restricted to the engineering theory of creep for metals in which it is assumed that the material does not possess any memory. This characterization of creep behaviour has very much in common with the theory of plasticity. There, strain increments are considered only in respect to a monotonically increasing parameter instead of real physical time as in the case of creep. In the following it is supposed that there is no interaction between the time independent plastic deformations which are thought of as occurring instantaneously, and the creep deformations developing during a time interval. It should be emphasized that this working hypothesis of no coupling between plastic and creep deformation is open to questions. In the formulation of a unified theory [22, 23] for rate sensitive dissipative processes the uncoupled engineering theories of creep and plasticity play the role of two extreme abstractions; but at the present it is only for those that quantitative experimental data are available which can be used in structural analysis.

The total deformation rate $\dot{\gamma}$ can be decomposed into instantaneous and time dependent components

$$\dot{\gamma} = \dot{\varepsilon} + \dot{\eta}_p + \alpha \dot{T} + \dot{\eta}_c \tag{92}$$

In contradistinction to the plastic strain-rate $\dot{\eta}_p$ which is derived from the current state variables T, σ or γ and their time derivatives, the creep strain-rate $\dot{\eta}_c$ is fully defined by the state of temperature T, stress σ and a hardening parameter as shown below. The creep strain-rate forms hence a prescribed initial strain-rate similar to that due to temperature changes.

Corresponding to plasticity it is assumed that only deviatoric components contribute to the energy dissipation in case of creep in metals. Hence, the von Mises yield criterion and the Prandtl-Reuss flow rule provide a consistent tool to describe the energy dissipation of the tensor field variables by equivalent uniaxial quantities, see equations (75), (77), (79).

Equivalent stress $$\bar{\sigma}^2 = \frac{3}{2}\, \sigma_D^t \sigma_D$$

Equivalent creep strain-rate $$\dot{\bar{\eta}}_c^2 = \frac{2}{3}\, \dot{\eta}_c^t \dot{\eta}_c \tag{93}$$

Flow rule $$\dot{\eta}_c = \dot{\bar{\eta}}_c\, s \qquad \text{where} \qquad s = \frac{3}{2\bar{\sigma}}\, \sigma_D$$

The question remains then how to compute the effective creep strain-rates $\dot{\bar{\eta}}_c$ for transient stresses and temperature conditions. In the following development attention is restricted to the description of uniaxial creep which can be extended to multi-axial states over the mechanism of equivalent stresses and strains.

In the present approach it is assumed that there exists a mechanical equation of state which describes the creep rate of the solid as a function of state variables [24,25,26]

$$\dot{\eta}_c = f(\sigma, T, t, \eta_c) \tag{94}$$

This equation implies that at any given time t the creep rate depends on the current state of the system and is independent of the path or previous history. However, similar to the problems arising in context with the deformation theory of plasticity there is conclusive evidence that the creep rate $\dot{\eta}_c$ does also depend on history of stress, deformation and temperature, hence the memory theory of viscoelastic-plastic solid would form a more appropriate way to describe this type of material response. The question arises then how the creep data, obtained from constant stress and temperature experiments, could be used for the case of time-varying stresses and temperatures. Different cumulative creep theories have been proposed; however, only the well-known time-hardening and strain-hardening rules are considered below.

Time-Hardening Law

The time-hardening rule assumes that the creep rate depends only on the current stress, the current temperature and the time from the beginning of the creep process. The creep rate at any instant of time is then defined by the following equation of state

$$\dot{\eta}_c = f(\sigma, T, t) \tag{95}$$

The creep strain may be frequently written as a power function of time

$$\eta_c = f_1(\sigma)\, f_2(T)\, t^{\rho} \tag{96}$$

such that

$$\dot{\eta}_c = f_1(\sigma)\, f_2(T)\, \rho\, t^{\rho-1} \tag{97}$$

Note that for secondary creep, where $\rho = 1$, the creep rate remains constant in time.

Strain-Hardening Law

The strain-hardening rule assumes that the creep rate depends only on the current stress, the current temperature and the accumulated creep strain. The creep rate at any instant of time is then defined by the following equation of state

$$\dot{\eta}_c = f(\sigma, T, \eta_c) \tag{98}$$

Elimination of the time t from equation (96) and (97) leads to the creep rate expression below

$$\dot{\eta}_c = \rho \left[f_1(\sigma)\, f_2(T) \right]^{1/\rho} \eta_c^{(\rho-1)/\rho} \tag{99}$$

Note that for secondary creep, the time-hardening and the strain-hardening method yield identical formulae. Fig. 26 illustrates the difference of both hardening rules for a varying stress and temperature conditions at time $t = t_1$. Although experimental data rather supports the strain-hardening rule, this method may lead to difficulties in describing creep during unloading if the accumulated creep strain is large. Hence, the simpler time-hardening method

is generally favoured for numerical calculations involving primary creep. For multi-axial conditions the rate of creep strain components are determined from equation (93) simply by substituting for $\dot{\eta}_c$ either the time-hardening or the strain-hardening laws of equations (97) or (99)

$$\dot{\eta}_c = \begin{cases} \{ f_1(\sigma)\, f_2(T)\, p\, t^{p-1} \}\, s & \text{Time-hardening} \\ \{ p\, [f_1(\sigma)\, f_2(T)]^{1/p}\, \dot{\eta}_c^{(p-1)/p} \}\, s & \text{Strain-hardening} \end{cases} \tag{100}$$

The final rate formulation of an isotropic solid exhibiting elastic, plastic, thermal and creep effects can now be written as

$$\begin{aligned} \dot{y} &= \dot{e} + \dot{\eta}_p + w\dot{T} + \dot{\eta}_c \\ &= E^{-1}\left(I + \frac{2G}{J} s s^t\right)\dot{\sigma} + (\gamma s + \alpha)\dot{T} + \dot{\eta}_c s \end{aligned} \tag{101}$$

An extension of the inverse relationship, equation (88), yields the following expression for the effective stress rate

$$\dot{\sigma} = E\dot{e} = F\dot{y} + G\dot{T} - \dot{\eta}_c E s \tag{102}$$

For the definition of the tangential material properties F and G see equation (90) and (91). It should be emphasized again that the creep rate components have to be considered prescribed, since they are determined from the existing state of stress, temperature and time or equivalent creep strain and not from their time derivatives.

c) Numerical Implementation

The finite element analysis of the transient thermal problem involving plasticity and creep requires the treatment of a set of coupled first order differential equations. With the help of incremental methods this problem reduces to the solution of algebraic equations. Euler's algorithm forms a very simple procedure in which the information at the beginning of each time step is used for the incremental treatment of the differential equations. There are various alternatives possible, such as the modified Euler method or the improved Euler method besides the more sophisticated multistep time integration algorithms; however, the latter are unpractical as they create considerable storage problems and require a certain degree of smoothness of the state variables with time. The following discussion is restricted to simple incremental strategies for solving the quasistatic equilibrium equations. To this end the differential stress-strain relation (102), is recast into an incremental form for the finite time interval $t, t+t_\Delta$. The resulting equilibrium equation may then be written as

$$(K + K_\Delta)(t)\, r_\Delta(t) = R_\Delta(t) + R_{p\Delta}(t) + R_{\theta\Delta}(t) + R_{c\Delta}(t) \tag{103}$$

The incremental tangent stiffness $K_\Delta(t)$ may arise from the temperature dependent material properties under transient conditions as well as from the non-linearity due to plasticity. The increments of prescribed initial loads due to temperature $R_{\theta\Delta}(t)$ and due to creep $R_{c\Delta}(t)$ can be evaluated directly from (19) for the given thermal condition and the mechanical state at the beginning of each time interval. These prescribed initial loads are simply added to the mechanical loading. The increment of the "instantaneous" plastic loads $R_{p\Delta}(t)$ arises either due to the temperature dependence of the hardening law in case of the direct "tangential stiffness" approach for the solution of the thermo-plastic problem, or altogether from the iterative treatment of the plasticity problem using initial load techniques.

The tangential stiffness method involves the repeated formation and decomposition of the structural stiffness matrix for each time increment, a rather costly strategy. Due to the finite size of the time interval further refinement is mostly required to avoid accumulation of linearization errors, hence multistep methods or equivalent iterations need to be employed together with equilibrium corrections before the beginning of a new time step. In case of temperature-independent properties modification techniques provide a very useful tool to account for localized plastifications. They furnish directly the desired information on changes of the results due to single changes in the stiffness without requiring the new formation and decomposition of the stiffness matrix [38, 39]. In case of temperature-dependent elastic properties under transient conditions the stiffness changes are not restricted to small areas, hence the modification procedures hardly apply. In case that the elastic properties remain independent of time equation (103) can be recast into the following form

$$K\, r_{\Delta}(t) = R_{\Delta}(t) + R_{p\Delta}(t) + R_{e\Delta}(t) + R_{c\Delta}(t) \qquad (104)$$

Creep and temperature only give rise to prescribed initial loads which add to the mechanical load increments. The non-linearity due to plasticity is treated using initial loaditeration in order to avoid the new formation and decomposition of the structural stiffness. This procedure accommodates a time variable system, in which the loading accounts for the time change of the structure due to creep and temperature dependent hardening as well as for the instantaneous changes due to plasticity [29, 30, 31, 32, 33, 34, 36, 37, 38].

As mentioned above the formulations of the plastic flow rule in equations (83) and (87) lead to two alternative initial load schemes for the iterative treatment of the incremental plasticity problem.

"Initial Strain Method"

For the initial strain approach the plastic strain increments are defined in terms of the increment of the elastic energy of distortion and in terms of the temperature increments, see equation (83). These plastic strain increments $\dot{\eta}_p$ are then utilized to construct the initial load increment $\dot{J}_\eta$ leading to an iterative process, since the current stress increments are not known a priori [38]. Fig. 27 a illustrates this formulation for the one-dimensional case. If convergence can be assured at all, this method provides better rates of convergence than the alternative initial stress approach; on the other hand, the initial strain method breaks down in case of non-hardening materials, where $\xi = 0$.

"Initial Stress Approach"

For the initial stress approach the plastic strain increments are defined in terms of the total energy of distortion and in terms of the temperature increments, see equation (87). These plastic strain increments $\dot{\eta}_p$ are then utilized to construct the initial load increment $\dot{J}_\eta$ leading to an iterative process, since the current total strain increments are not known a priori. Fig. 27 b illustrates this formulation for the one-dimensional case. This procedure was presented first in form of initial stresses in [37]. Note that the expression for the flow rule (87) clearly indicates that this method also applies to non-hardening plastic material where $\xi=0$; hence this formulation enlarges considerably the range of convergence in comparison to the associated initial strain approach. It is interesting to note that the differences between the initial stress and initial strain schemes arise solely from the alternative descriptions of $\dot{\eta}_p$ in equation (82) and (86).

For a detailed theoretical discussion of the numerical implications, such as range and rate of convergence, the reader is referred to [38], in which the iterative initial load techniques are investigated. Basically, three methods may be distinguished which are denoted in short by DIM, the direct incremental method, NIM, the normal iterative method, and VIM, the improved iterative method. DIM is based solely on load incrementation without iteration where the magnitudes of the current elastically suppressed plastic strains are estimated directly from the previous load increment. NIM incorporates additionally within each load increment an iterative scheme accounting for the error made due to the finite size of the load increment. VIM is a Newton-Raphson procedure applied to the plastic variables in order to accelerate the convergence properties of NIM. A schematic representation of these initial load techniques is given in Fig. 28 [35, 36, 38]. It should be mentioned that none of these methods alters the initial elastic stiffness.

In the following the results of two elasto-plastic problems are presented to illustrate these iterative schemes. The number of iterations necessary to achieve a preset accuracy of plastic strains or stresses is of particular interest, as it gives an indication of the range and rate of convergence for the individual methods. The first example deals with the elasto-plastic analysis of the statically indeterminate truss, illustrated in Fig. 29, while the second one involves the rectangular membrane with central crack, shown in Fig. 30. For both cases a modification of the Ramberg-Osgood equation describes the uniaxial stress-strain law

$$\eta = \frac{1.1\,\sigma_y}{m\,E}\left[\left(\frac{\sigma}{1.1\,\sigma_y}\right)^m - \left(\frac{1}{1.1}\right)^m\right] \qquad (105)$$

The following material constants are chosen to characterize the aluminium alloy 2024-T3: Young's modulus $E = 11.4 \times 10^6$ lbf/in^2, initial yield stress $\sigma_y = 34\,500$ lbf/in^2, exponent $m = 10$ and elastic Poisson's ratio $\nu = 0.3$. An elastic solution determines the loading at which local yielding occurs first while the subsequent load increments are described by the non-dimensional scalar load factor λ which is incremented by $\lambda_\Delta = 0.1$.

Discussion of Results:

Tables 2 and 3 summarize the results of the elasto-plastic analyses of both structures shown in Fig. 29 and 30. Both tables present the number of iterations necessary to obtain a relative error e less than 10^{-4} for the equivalent plastic strain-rates in equation (82) or (86), where

$$e = \frac{|\dot{\bar{\eta}}_i - \dot{\bar{\eta}}_{i-1}|}{\max(\dot{\bar{\eta}}_{i-1})} = \frac{|\Delta\dot{\bar{\eta}}_i|}{\max(\dot{\bar{\eta}}_{i-1})} < 10^{-4} \qquad (106)$$

In addition the maximum equivalent stress is given for each loading step λ. Both iterative procedures, NIM and VIM, are applied to the initial stress and initial strain formulation of the non-linear elasto-plastic problem.

Table 2 presents the results for the simple truss of Fig. 29 verifying the theoretical predictions made in [38] in regard to the convergence properties of the normal iterative method. The range of convergence of NIM is larger when the initial stress formulation is used versus the initial strain formulation, which diverges already at $\lambda = 1.5$. However, if it converges at all, the initial strain formulation converges faster. Moreover, VIM, the Newton-Raphson modification of NIM, improves considerably the rate of convergence if applied to both, the initial stress and initial strain approach. It should be noted that in case of VIM and initial strain, the range of convergence is also considerably enlarged in comparison to NIM.

Load-factor λ	Maximum Effective Stress $\bar{\sigma}_{max}$ [lbf/in^2]	Initial Stress Approach		Initial Strain Approach	
		NIM	VIM	NIM	VIM
1.0	34500	-	-	-	-
1.1	36930	5	4	22	5
1.2	38980	5	4		4
1.3	40690	7	4		5
1.4	42180	6	5		5
1.5	43450	5	4		5
1.6	44550	5	5		5
1.7	45520	5	5	Divergence	5
1.8	46390	7	5		5
1.9	47170	8	5		5
2.0	47880	7	5		5

Table 3 Rectangular Membrane with Crack - Number of Iterations for Relative Error of Plastic Strains $< 10^{-4}$

Load-factor λ	Maximum Effective Stress $\bar{\sigma}_{max}$ [lbf/in^2]	Initial Stress Approach		Initial Strain Approach	
		NIM	VIM	NIM	VIM
1.0	34500	-	-	-	-
1.1	37730	10	4	6	3
1.2	40740	12	3	6	3
1.3	43460	15	3	9	3
1.4	45890	20	3	17	3
1.5	48120	26	3		2
1.6	50240	35	3		2
1.7	52370	53	3		2
1.8	51620	79	3		3
1.9	57040	116	3	Divergence	3
2.0	59610	163	3		4

Table 2 Indeterminate Truss - Number of Iterations for Relative Error of Plastic Strains $< 10^{-4}$

Table 3 presents the results of the rectangular membrane with central crack illustrated in Fig. 30. The comparison for this structure agrees very well with the theoretical predictions made in [38]. NIM-initial stress now requires far less iterations than in the case of the truss. Only at relatively high loads the number of iterations can be markedly reduced by the application of VIM. Whilst NIM-initial stress converges more quickly when the number of constraints is greater, the converse is true for NIM-initial strain. Even for $\lambda = 1.1$ there are 22 iterations necessary and divergence occurs already for $\lambda = 1.2$. Note that VIM-initial strain requires in most loading steps the same number of iterations as VIM-initial stress.

In conclusion it can be stated that VIM improves considerably the range of convergence of the initial strain approach as well as the rate of convergence for structures with few kinematic constraints. In case of continuum problems the initial stress formulation seems to be suited best for automatic computations. It should be mentioned that the improved iterative method VIM is considerably more costly per iteration than NIM depending on the number of Newton-variables involved. An optimum approach in regard to computational effort is adopted if Newton variables are considered only above a certain threshold.

Two more remarks may be pertinent to the discussion of different initial load techniques: the first concerns the treatment of thermo-elasto-plastic problems under transient temperature conditions, while the second deals with the choice of time steps for the creep analysis. From equation (80) one can see that there are two sources for plastic loading in the case of transient temperature distributions, the customary mechanical source due to the change of equivalent stress $\dot{\bar{\sigma}}$ and the thermal source due to changes of temperature $\dot{T}$. Fig. 25 a illustrates the two paths which are possible for transient temperature conditions. It clearly indicates that very large increments of plastic strains are to be expected for temperature loading, path O-A, leading to numerical stability problems particularly for materials with little strain-hardening. On the other hand, unloading due to a temperature decrease from T_2 to T_1 is simply accounted for by increasing the current $\bar{\sigma}_{max}$ corresponding to point O by the value at B. It should be mentioned that a similar phenomenon occurs in the case of primary creep analysis if cyclic loading is dealt with by the strain-hardening method. There unloading is being presented by path A-O in Fig. 26 a, where O may not be reached any more if sufficient strain-hardening has preceded unloading.

The last comment pertains to the choice of time steps used in the creep analysis. Here the same stability problems occur as in the classical numerical treatment of plasticity problems with the aid of the direct incremental method, denoted above by DIM. Experience has indicated that the increments of creep strains should be less than the elastic strains to insure stability, see also [29]

$$\dot{\bar{\eta}}_c < \mu \bar{\varepsilon} = \mu \frac{\bar{\sigma}}{E} \qquad \text{with} \qquad 0 \leq \mu \lesssim 0.25 \tag{107}$$

For numerical computations the simplest method is to derive from the prevailing state of elastic strain an admissible increment of creep strains which can be easily transformed into a physical time step via equation (97). It should be emphasized again that there is a basic difference between plastic and creep strain increments due to the homogeneous and non-homogeneous definition of these quantities. Iterative techniques similar to NIM and VIM do not apply to the virtual work formulation of the creep problem in which it is tacitly assumed that the state of stress or total strain remains constant within a given time interval for the rate of creep or corresponding relaxation method. To this end an extension of the Hellinger-Reissner variational principle [25], [28] could provide an alternative platform to deal in a more efficient way with the creep analysis of structures.

d) Example

A realistic thermal stress analysis is performed with the help of the initial load technique on a spherical pressure vessel with radial nozzle. The inside of the vessel is subjected to a sudden temperature rise for which the steady state temperature distribution is first determined. Subsequently, the instantaneous thermo-elasto-plastic stress distribution is evaluated for the vessel accounting for temperature dependent material properties. Thereafter, the stress redistribution due to creep is traced as function of time. Finally, in addition the elasto-plastic stress analysis is carried out for internal pressure under which limit design would predict partial collapse.

The meridional section of the structure is idealised by 230 axisymmetric TRIXC6 elements resulting in 551 nodal points. The same discretisation is employed for both, the temperature and the subsequent stress analysis, see Fig. 31.

The thermal boundary value problem is defined for the steady state case as follows. The inside surface of the vessel is subjected to a prescribed temperature of 250° C, while the ambient air temperature on the outside is 20° C. The upper surface of the nozzle flange and the bottom rim of the idealised structure are insulated against heat flow.

The following thermal material properties are chosen:

Thermal conductivity $k = 0.398$ kcal/cmh °C

Specific heat $c = 0.114$ kcal/kg °C

Heat transfer coefficient between the outside surface of the vessel and the air

$h = 0.0426$ kcal/cm^2 h °C

Density $\varrho = 7.9 \times 10^{-3}$ kg/cm^3

Fig. 33 illustrates the resulting steady state temperature distribution in form of contour lines.

For the subsequent mechanical analysis of the structure the material constants are taken for mild steel where the elastic properties are defined as

$$E = 21000 \ \text{kp/mm}^2 \qquad \text{and} \qquad \nu = 0.30$$

The coefficient of thermal expansion is assumed to be temperature dependent

$$\alpha = \alpha_{10} - (\alpha_{10} - \alpha_0)\left(1 - \frac{T}{T_1}\right)^2 \tag{108}$$

where

$$\alpha_0 = 1.0 \times 10^{-5} \ 1/^\circ\text{C}$$

$$\alpha_{10} = 1.7 \times 10^{-5} \ 1/^\circ\text{C}$$

$$T_1 = 720^\circ\text{C}$$

and its variation is accounted for during the course of incremental loading which is required for the thermo-elasto-plastic stress analysis.

In the plastic range a Ramberg-Osgood type stress-strain law as given in Equation (105) is used. The temperature dependence of the yield stress is described by

$$\sigma_y = \sigma_{y_0}\left[1 - \left(\frac{T}{T_0}\right)^2\right] \tag{109}$$

where

$$\sigma_{y_0} = 26 \ \text{kp/mm}^2$$

$$T_0 = 850^\circ$$

$$m = 20 \qquad \text{see Equation (105)}$$

Fig. 32 shows the unaxial stress-plastic strain relationship as function of the temperature.

The incremental procedure starts from a stress free reference state with applying a fraction of the steady state temperature distribution for each loading step. The final temperature condition is reached after 13 increments. Subsequently, the stepwise calculation is continued to account for secondary creep effects. The following creep law given in [24] is chosen to compute the initial creep strain increment at each time step

$$\eta_{c\Delta} = \left(\frac{\bar{\sigma}\ [\text{kp/mm}^2]}{2390}\right)^{6.5} \frac{t\ [\text{sec}]}{10^9}\ \mathbf{s}\ ; \qquad \mathbf{s} = \frac{3}{2\bar{\sigma}}\,\boldsymbol{\sigma}_D \tag{110}$$

The time interval was automatically adjusted such that the change of the maximum equivalent stress occurring in the structure never exceeded 5% of the instantaneous maximum equivalent stress. The procedure was terminated after 21 increments which corresponds to a time of 181 days.

Fig. 34, 35 and 36 illustrate the resulting stress distributions. One observes that the plastic zones (shaded areas) develop first at the inside of the flange. This may be explained by the relatively low temperature at the outside of the flange which prevents the expansion of the hot inner portion and thus induces large compressive hoop stresses. Plastification of the inter-

section between the nozzle and the sphere, where pronounced stress concentrations occur, starts only at a later loading stage. Note that in the case of a temperature dependent yield surface the maximum equivalent stress is not alone responsible for plastic flow, but rather a combination of the state of stress and temperature. Figs. 35 and 36 illustrate the stress relaxation due to creep causing a significant redistribution of stresses in the flange.

For comparison, the spherical shell with nozzle is also subjected to a monotonically increasing pressure whereby the temperature and creep effects are disregarded. Fig. 37 shows the equivalent stress distribution for the pressure $p = 33.4\ kp/cm^2$ at the beginning of plastification. The internal pressure is further increased to $90.2\ kp/cm^2$ for which the theory of limit design predicts a collapse mechanism at the junction between the nozzle and the sphere. The stress distribution for this limit pressure, which is attained after 17 loading steps, is shown in Fig. 37. It once again indicates that limit design procedures yield but a conservative lower bound.

In conclusion one may state that an important class of thermomechanical problems can be solved, accounting for plasticity as well as creep by the initial load technique without altering the initial stiffness. The extension of this type of analysis to transient temperature conditions may seem trivial, but experience has shown that particularly the temperature dependence of the yield surface in general leads to serious convergence problems of the iterative scheme, especially if there is little strain hardening. Particular care has to be exercised in choosing an appropriate time-step for the associated heat conduction analysis in order to avoid any spurious oscillation of the temperature evolution in time and to keep small the plastic loading term due to temperature changes.

VI ACKNOWLEDGEMENTS

This paper summarizes some results of an investigation into the finite element analysis of thermal stress problems. This research has been supported by a number of organisations, including the "Bundesministerium für Bildung und Wissenschaft" (grant SBB 4), Bonn.

The authors wish to thank all members of the ISD for their continuous support in the preparation of this paper; in particular the advice and help by Dr. K.E. Buck is gratefully acknowledged.

VII. REFERENCES

[1] Fung, Y.C., Foundations of Solid Mechanics, Englewood Cliffs, N.J.: Prentice-Hall Inc., 1965.

[2] Parkus, H., Thermoelasticity, Blaisdell Publ.Co., Waltham, Mass., 1968.

[3] Nickell, R.E. and Sackman, J.L., Approximate Solutions in Linear, Coupled Thermoelasticity, J. Appl. Mech., June 1968.

[4] Chao-Hwang Lu, Nonlinear Theory of Thermoelasticity, Ph.D. Dissertation to Division of Structural Engineering and Structural Mechanics, University of California, Berkeley, 1971.

[5] Oden, J.T., and Kross, D.A., Analysis of General Coupled Thermoelasticity Problems by the FEM, Proc. 2nd Conf. on Matrix Methods in Struct. Mech., Wright-Patterson Air Force Base, Ohio, 1968.

[6] Zienkiewicz, O.C. and Cheung, Y.K., Finite Elements in the Solution of Field Problems, The Engineer, Sept. 1965.

[7] Wilson, E.L. and Nickell, R.E., Application of the FEM to Heat Conduction Analysis, Nuclear Eng. and Design, 4, 1966.

[8] Visser, W., A FEM for the Determination of Non-stationary Temperature Distributions and Thermal Deformations, Proc. 2nd Conf. on Matrix Methods in Struct. Mech., Wright Patterson Air Force Base, Ohio, 1965.

[9] Argyris, J.H., Brönlund, O.E., Fried, I., and Spooner, J.B., The Changes in the Stress Distribution round a Rectangular Hole with Rounded Corners, Caused by a Varying Internal Pressure and Temperature, Conf. of the Int. Astron. Fed., Belgrade, 1967.

[10] Argyris, J.H. and Mareczek, G., Thermomechanical Analysis of Structures, to be presented to the 4th Conf. of the Hung. Acad. of Sciences on Dimensioning and Strength Calculations, Budapest, October 1971.

[11] Argyris, J.H., Energy Theorems and Structural Analysis, Aircraft Eng. 26, 1954 27, 1956. Also as book: Butterworths London, 1960.

[12] Melosh, R.J., Basis for Derivation of Matrices for the Direct Stiffness Method, AIAA J., 1, 1963.

[13] Argyris, J.H., Recent Advances in Matrix Methods of Structural Analysis, Pergamon Press, London, 1964.

[14] Argyris, J.H., Triangular Elements with Linearly Varying Strain for the Matrix Displacement Method, J. of the Roy. Aeron. Soc., 69, 1965.

[15] Argyris, J.H., The TRIAX6 Element for Axisymmetric Analysis by the Matrix Displacement Method, The Aeron. J. of the Roy. Aeron. Soc., 70, 1966.

[16] Sternberg, E., Transient Thermal Stresses in an Infinite Medium with a Spherical Cavity, Koninkl. Nederl. Akad. van Wetenschappen, Amsterdam, Proceed. B. 60, 1957.

[17] Nowinski, J., Transient Thermoelastic Problem for an Infinite Medium with a Spherical Cavity Exhibiting Temperature Dependent Properties, J. of Appl. Mech., June 1962.

[18] Everett, F.L. and Miklovitz, Poisson's Ratio at High Temperatures, J. of Appl. Phys., 15, 1944.

[19] Prager, W., Non-Isothermal Plastic Deformation, Proceed. Koninkl. Nederl. Akad. van Wetenschappen, Amsterdam, B. 61, 1958.

[20] Drucker, D.C., A Definition of Stable Inelastic Material, J. of Appl. Mech., 1959.

[21] Naghdi, P.M., Stress-Strain Relation in Plasticity and Thermo-Plasticity, in "Plasticity", Proc. 2nd Symp. on Naval Struct. Mech., Pergamon, 1963.

[22] Naghdi, P.M. and Murch, S.A., On the Mechanical Behaviour of Viscoelastic/Plastic Solids, Trans. ASME, Sept. 1963.

[23] Rice, J.R., On the Structure of Stress-Strain Relations for Time-Dependent Plastic Deformation of Metals, Trans. ASME, Sept. 1970.

[24] Hult, J., Creep in Engineering Structures, Blaisdell Publ. Co., Waltham, Mass., 1968.

[25] Rabotnov, Y.N., Creep Problems in Structural Members, North Holland Publ. Co., 1969.

[26] Mendelson, A., Plasticity: Theory and Application, The MacMillan Co., New York, London, 1968.

[27] Wang, A.J. and Prager, W., Thermal and Creep Effects in Work-Hardening Elastic-Plastic Solids, J. of Aeron. Sciences, May 1954.

[28] Pian, T.H.H., On the Variational Theorem for Creep, J. of the Aeronaut. Sciences, November 1957.

[29] Greenbaum, G.A. and Rubinstein, M.F., Creep Analysis of Axisymmetric Bodies Using Finite Elements, Nuclear Eng. and Design, 7, 1968.

[30] Gallagher, R.H., Padlog, J. and Bijlaard, P.P., Stress Analysis of Heated Complex Shapes. J. Am. Rocket Soc.,32, 1962.

[31] Argyris, J.H., Continua and Discontinua, Proc. 1st Conf. Matrix Methods Struct. Mech., Wright-Patterson Air Force Base, Ohio , 1965.

[32] Argyris, J.H., Elasto-Plastic Matrix Displacement Analysis of Three-Dimensional Continua. J. of the Roy. Aeron. Soc., 69, 1965.

[33] Argyris, J.H., Scharpf, D.W. and Spooner, J.B., Die elastoplastische Berechnung von allgemeinen Tragwerken und Kontinua, Ingenieur Archiv, Vol. 37, 1969.

[34] Argyris, J.H., Scharpf, D.W. and Spooner, J.B., The Elasto-Plastic Calculation of General Structures and Continua, Proceedings, 3rd Conference on Dimensioning, Budapest, 1969.

[35] Argyris, J.H., Buck, K.E., Scharpf, D.W., Hilber, H.M. and Mareczek, G., Some New Elements for the Matrix Displacement Method, Proc. 2nd Conf. Matrix Methods Struct. Mech., Wright-Patterson Air Force Base, Ohio, 1968.

[36] Scharpf, D.W., Die Frage der Konvergenz bei der Berechnung elastoplastisch deformierbarer Tragwerke und Kontinua, Dr. Ing. Thesis, University of Stuttgart, 1969.

[37] Zienkiewicz, O.C., Valliapan, S., King, I.P., Elasto-Plastic Solutions of Engineering Problems, Initial Stress, Finite Element Approach, Ing. J. Num. Meth. Eng., 1969.

[38] Argyris, J.H and Scharpf, D.W., Methods of Elastoplastic Analysis, Proc. of the ISD-ISSC Symp. on Finite Element Techniques, Institut für Statik und Dynamik der Luft-und Raumfahrtkonstruktionen, Stuttgart, 1969, also to be published in ZAMP.

[39] Roy, J., Allgemeine Modifikationsverfahren für die Lineare und Nichtlineare Berechnung von Tragwerken und Kontinua mit der Matrizenverschiebungsmethode, Dr. Ing. Thesis, to be submitted at the University of Stuttgart, 1971.

[40] Irons, B.M., Numerical Integration Applied to FEM, Int. Symp. on the Use of Electronic Digital Computers in Structural Eng. at the University of Newcastle upon Tyne, 1967.

[41] Ergatoudis, J., Irons, B.M. and Zienkiewicz, O.C., Curved, Isoparametric, Quadrilateral Elements for Finite Element Analysis, Int. J. Solids Structures, 7, 1968.

[42] Argyris, J.H. and Fried, I., The LUMINA Element for the Matrix Displacement Method, The Aeron. J. of the Roy. Aeron. Soc., 72, 1968.

[43] Argyris, J.H., and Scharpf, D.W., The Curved Tetrahedronal and Triangular Elements TEC and TRIC for the Matrix Displacement Method. Part I Small Displacements, Part II Large Displacements, The Aeron.J. of the Roy. Aeron.Soc., 73, 1969.

[44] Felippa, C.A., Refined Finite Element Analysis of Linear and Nonlinear Two-Dimensional Structures, UC-SESM Report No.66-22, University of California, Berkeley, October 1966.

[45] Willam, K.J., "Finite Element Analysis of Cellular Structures", Ph.D. Dissertation to Division of Structural Engineering and Structural Mechanics, University of California, Berkeley, 1969.

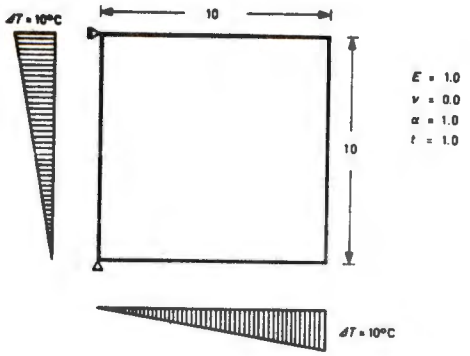

Fig.1 Quadratic Membrane
Description of "Residual Stress" Problem

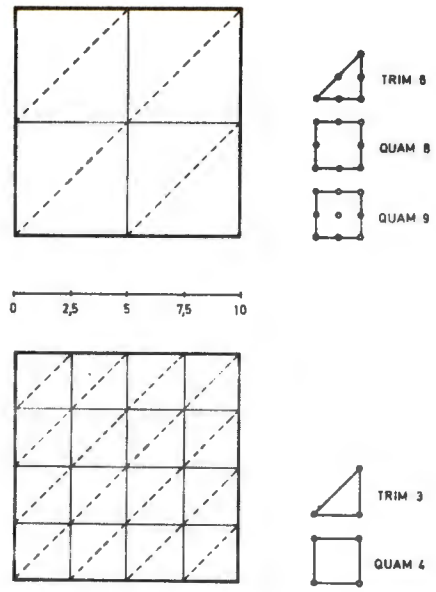

Fig.2 Discretisation of Phase I
"Constant" Jacobian

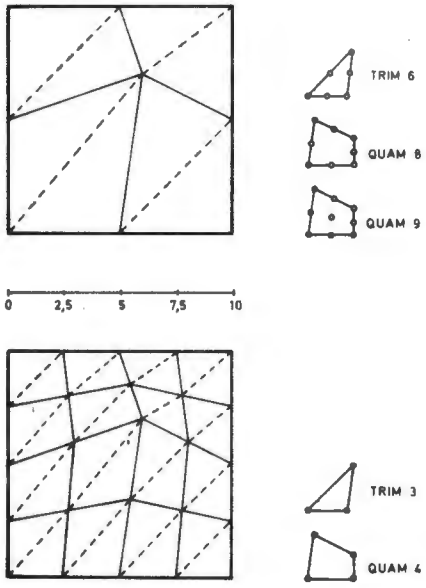

Fig.3 Discretisation of Phase II
"Linear" Jacobian

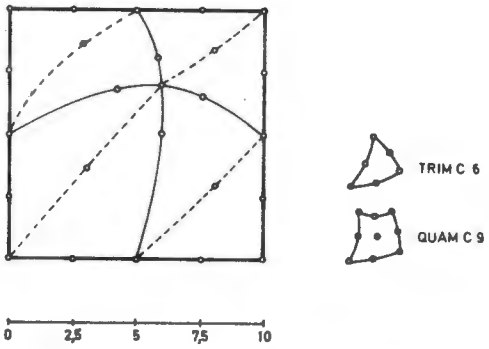

Fig.4 Discretisation of Phase III
"Quadratic" Jacobian

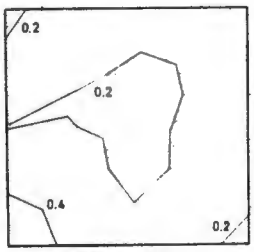

Distribution of τ_0

Fig.5 Phase II, Element TRIM 3

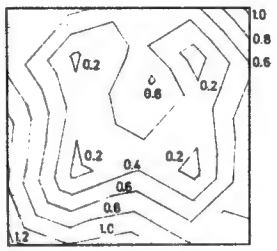

Distribution of τ_0

Fig.6 Phase II, Element QUAM 4

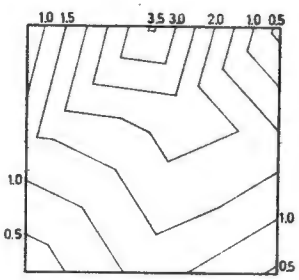

Distribution of τ_0

Fig.7 Phase III, Element TRIMC 6

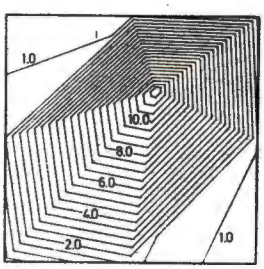

Distribution of τ_0

Fig.8 Phase III, Element QUAMC 9

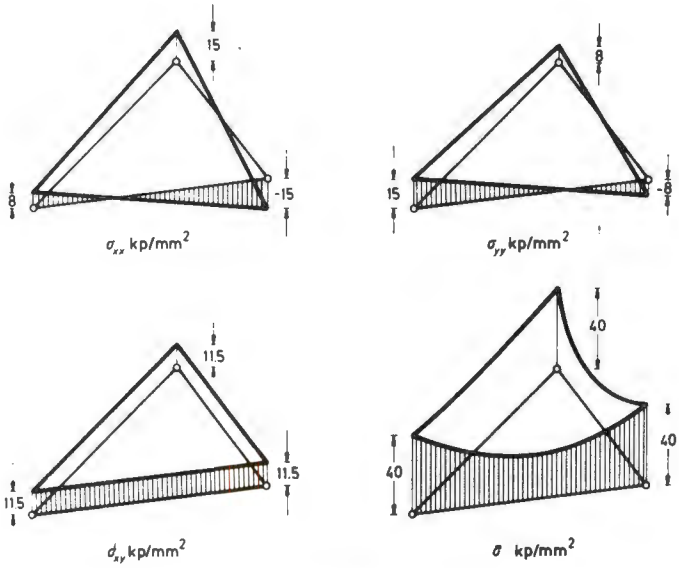

Fig.9 Stress Distribution

Deviatoric Components and Equivalent Stress

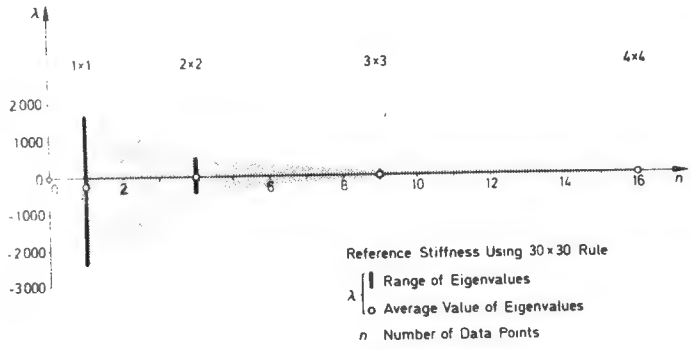

Fig. 11 Comparison of Elasto-Plastic Stiffness Matrices

Different Gaussian Quadrature Rules

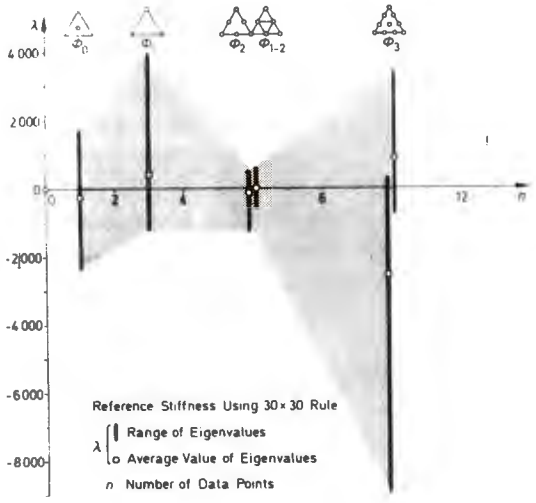

Fig. 13 Comparison of Elasto-Plastic Stiffness Matrices

Different Interpolation Schemes

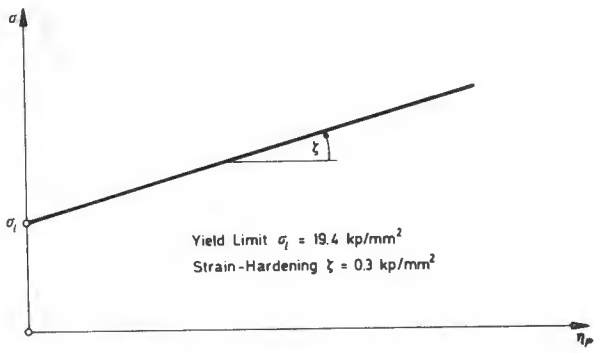

Fig. 10 Stress-Plastic Strain Relationship

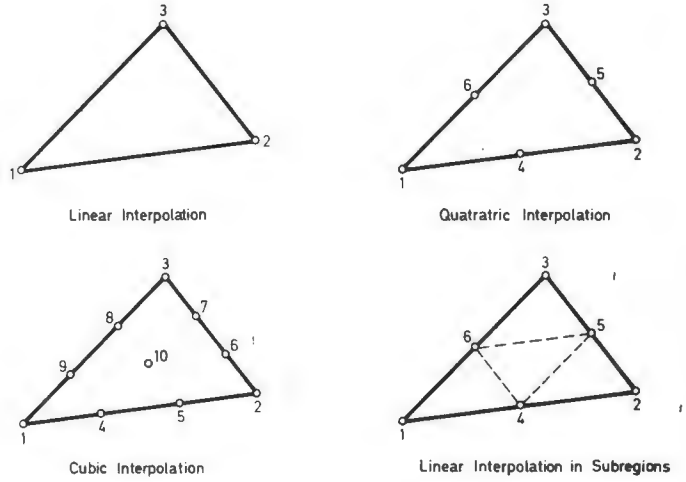

Fig. 12 Representation of Elasto-Plastic Material Properties

Linear Strain Triangle TRIM 6

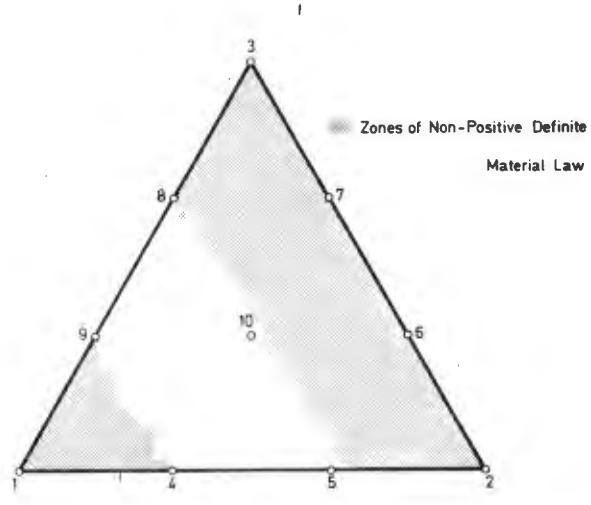

Fig. 14 Cubic Interpolation Scheme

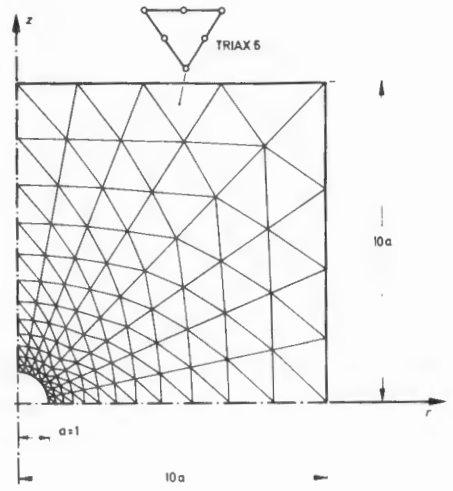

425 Nodal Points
192 TRIAX 6 Elements

Fig.16 Circular Cylinder with Spherical Cavity
Idealisation

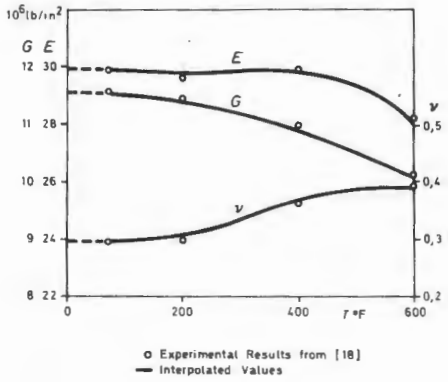

Fig.17 Temperature Dependence of Elastic Properties
Variation of E, ν and G

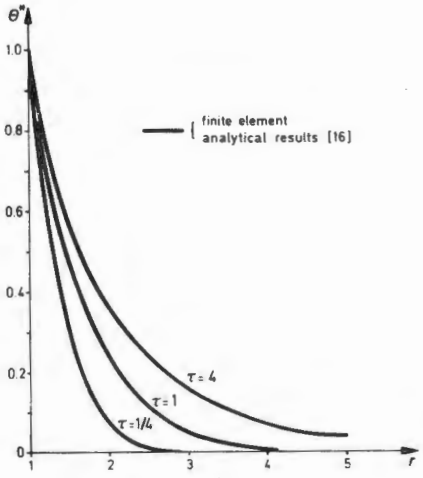

Fig.18 Transient Temperature
Radial Distribution at Different Times τ

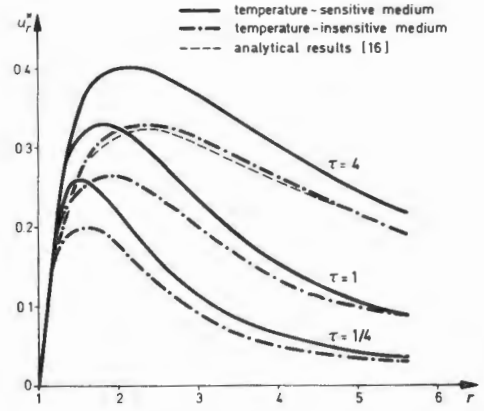

Fig. 19 Radial Displacements
Radial Distribution at Different Times τ

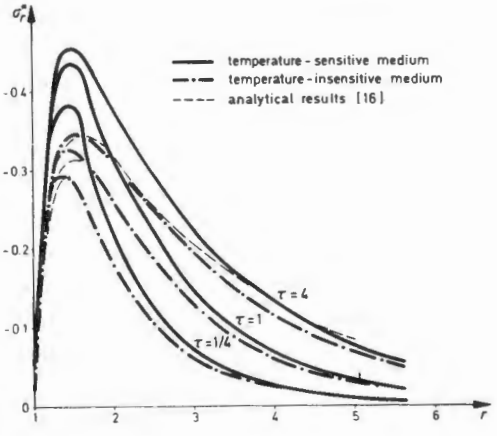

Fig.20 Radial Stresses
Radial Distribution at Different Times τ

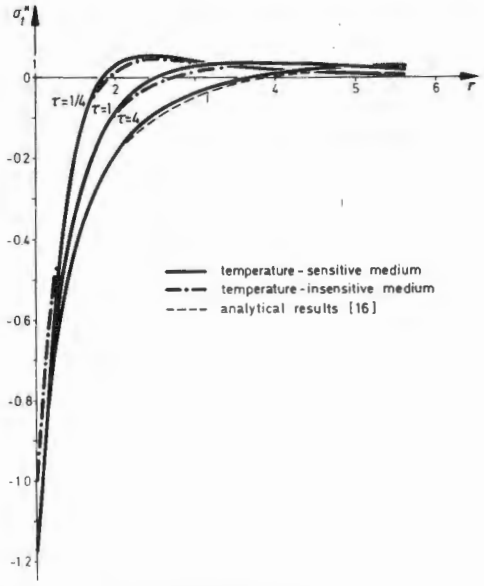

Fig.21 Tangential Stresses
Radial Distribution at Different Times τ

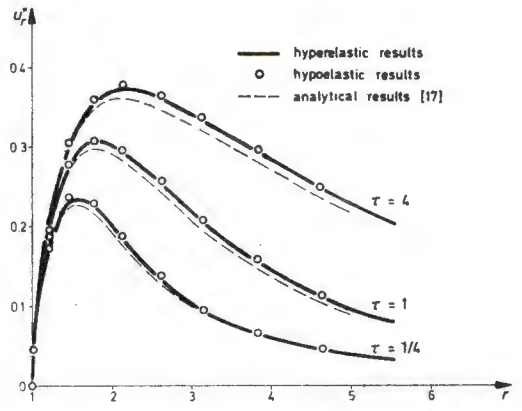

Fig. 22 Radial Displacements
Radial Distribution at Different Times τ

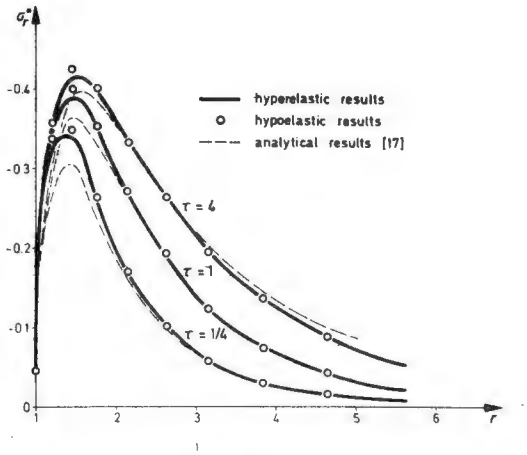

Fig. 23 Radial Stresses
Radial Distribution at Different Times τ

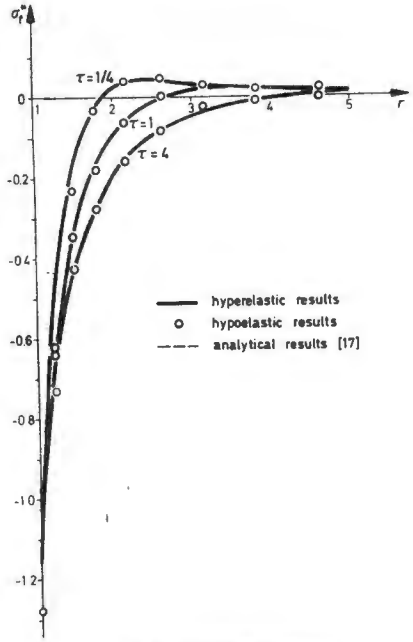

Fig. 24 Tangential Stresses
Radial Distribution at Different Times τ

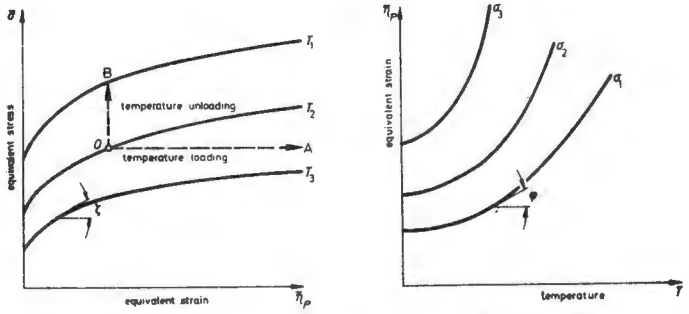

a) Definition of ζ

b) Definition of φ

Fig. 25 Temperature Dependent Workhardening Parameters

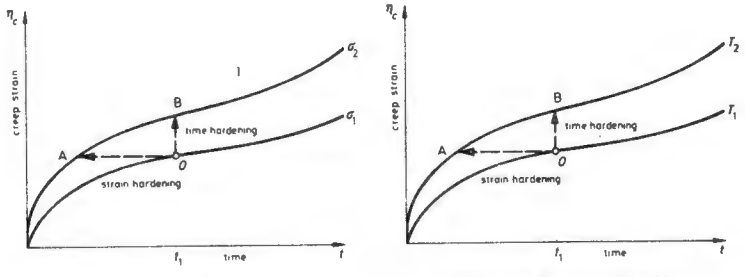

a) Variable Stress Conditions

b) Variable Temperature Conditions

Fig. 26 Transient Effects on Creep Rate

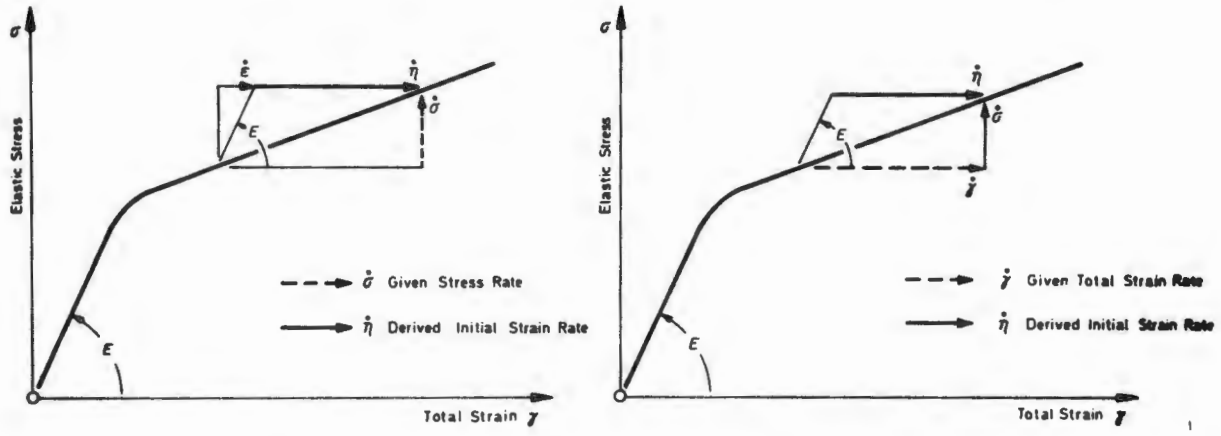

a) Initial Strain Approach

b) Initial Stress Approach

Fig. 27 Initial Load Methods

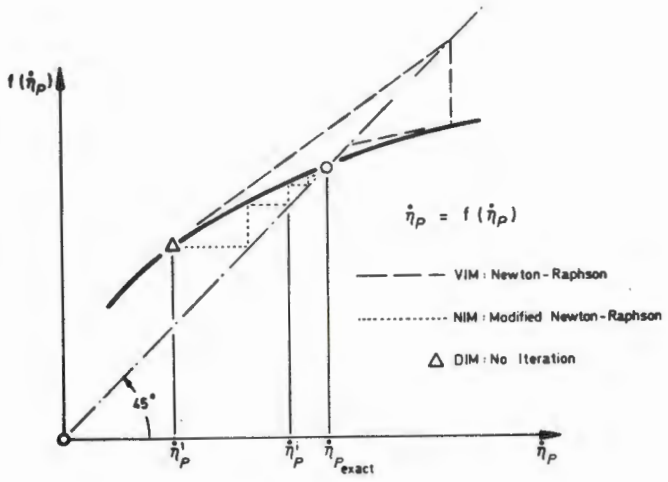

Fig. 28 Incremental Initial Load Methods

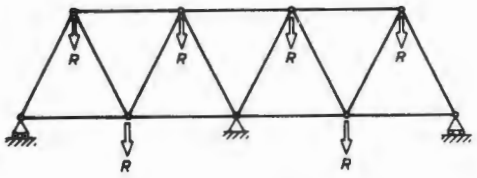

Fig. 29 Indeterminate Truss

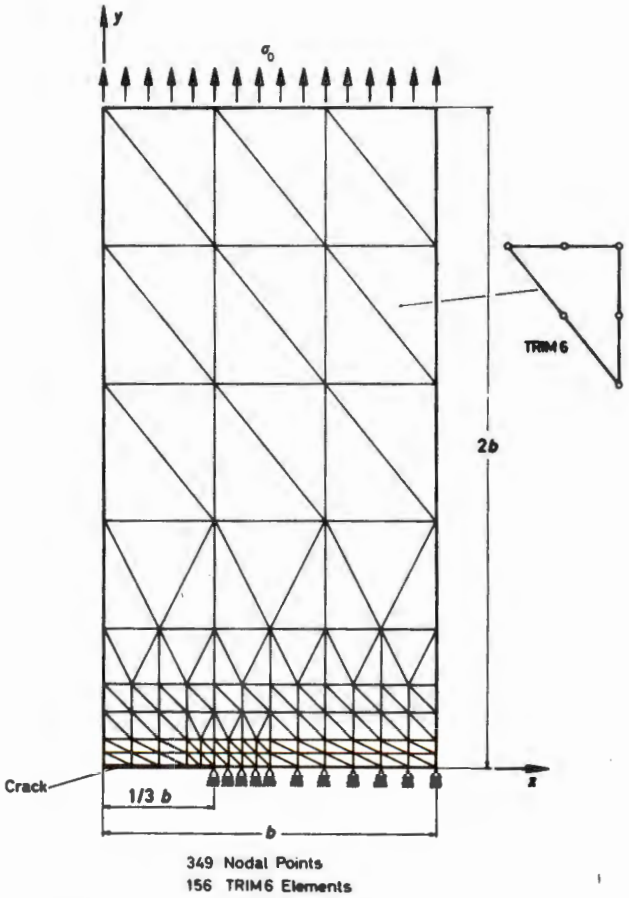

Fig. 30 Rectangular Membrane with Crack
Idealisation

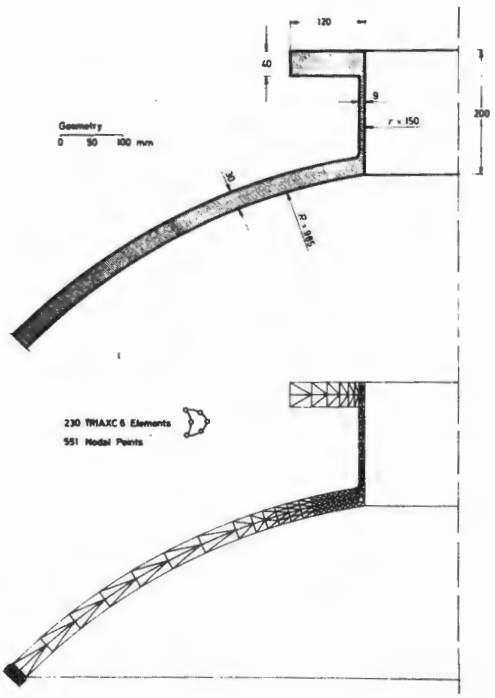

Fig. 31 Spherical Shell with Nozzle
Geometry and Idealisation

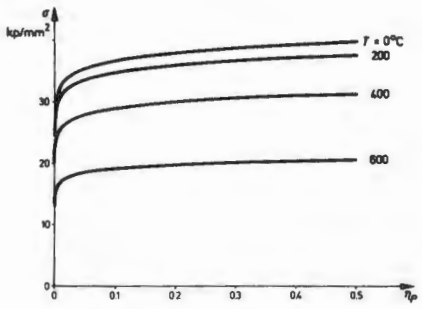

Fig. 32 Uniaxial Stress - Plastic Strain Properties

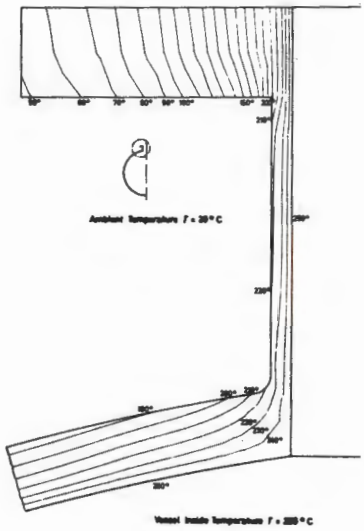

Fig. 33 Spherical Shell with Nozzle
Steady State Temperature Distribution

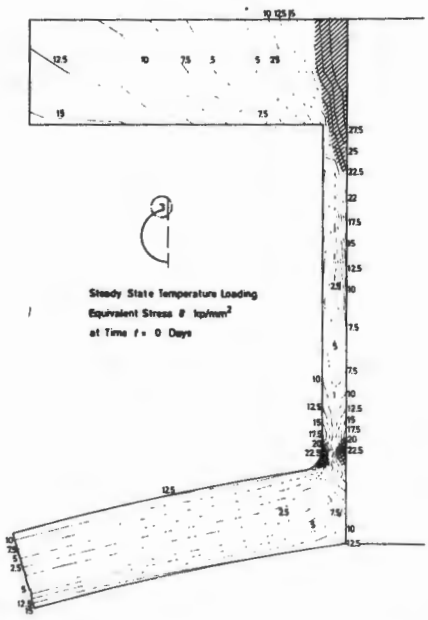

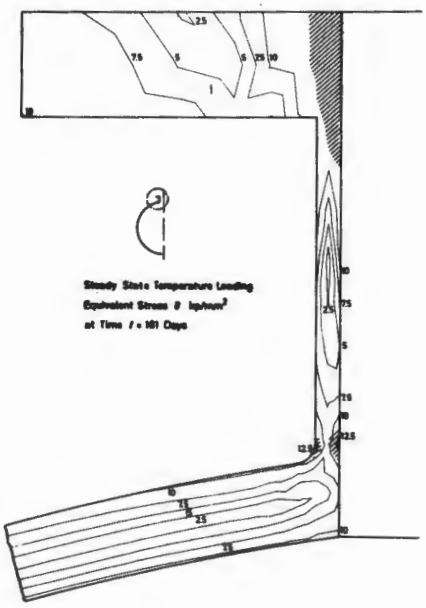

Fig. 34 Spherical Shell with Nozzle
Equivalent Stress Distribution

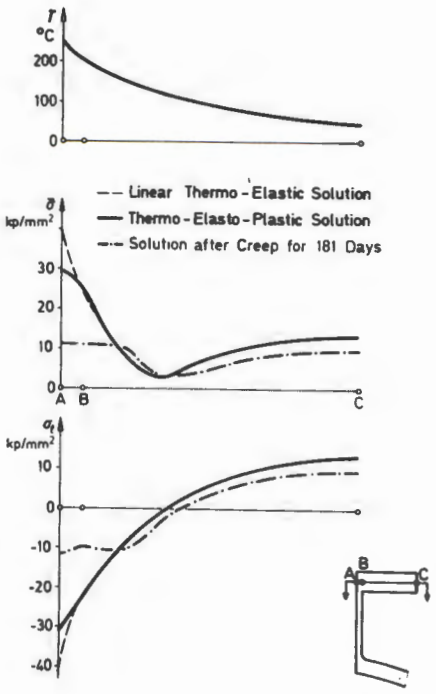

Fig. 35 Spherical Shell with Nozzle
Equivalent Stresses at Section A-C

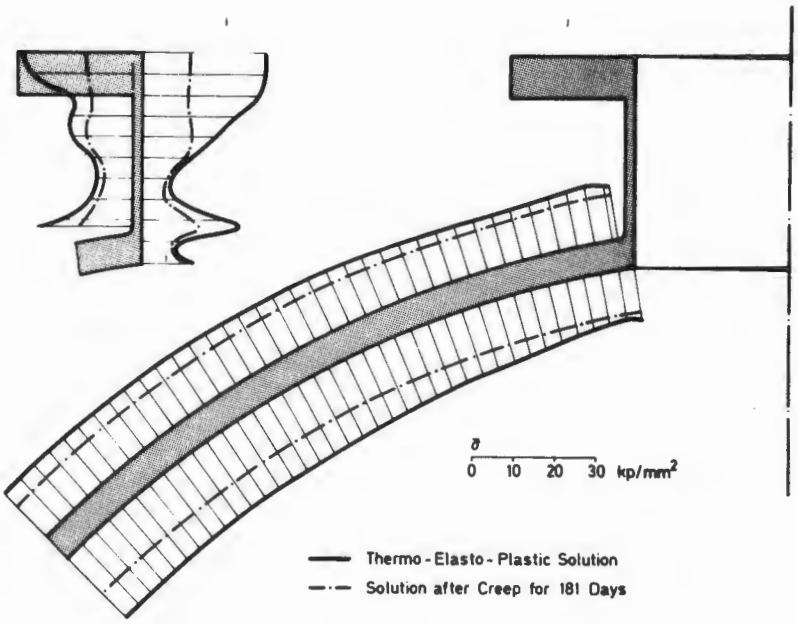

Fig. 36 Spherical Shell with Nozzle
Equivalent Stress Distribution

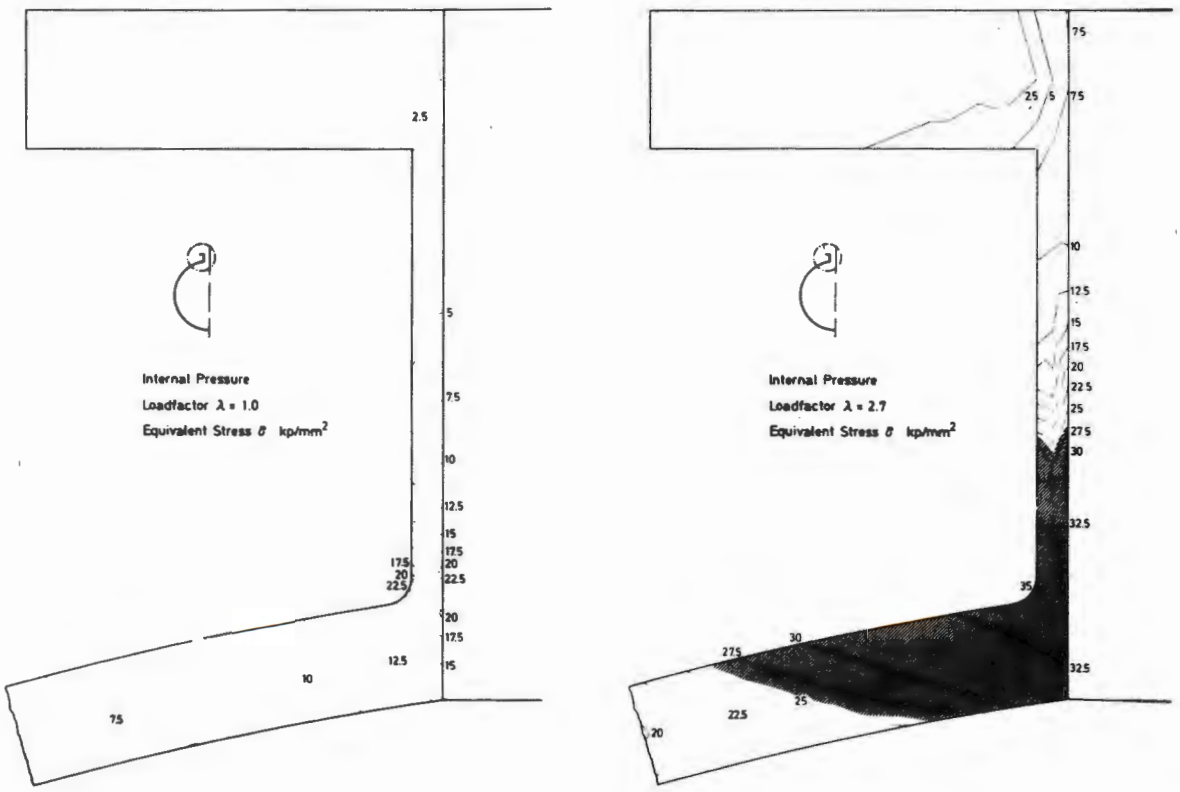

Fig. 37 Spherical Shell with Nozzle
Equivalent Stress Distribution